5-2019

In Vitro Simulation of Microgravity Induced Muscle Loss Successfully Increases Expression of Key In Vivo Atrophy Markers

Charles P. Harding
Utah State University

IN VITRO SIMULATION OF MICROGRAVITY INDUCED MUSCLE LOSS SUCCESSFULLY INCREASES EXPRESSION OF KEY IN VIVO ATROPHY MARKERS

by

Charles P. Harding

A thesis submitted in partial fulfillment

of the requirements for the degree

of

MASTER OF SCIENCE

in

Biological Engineering

Approved:

_____	_____
Elizabeth Vargis, Ph.D. Major Professor	Jon Takemoto, Ph.D. Committee Member
_____	_____
Timothy Taylor, Ph.D. Committee Member	Laurens H. Smith, Ph.D. Interim Vice President for Research and Dean of the School of Graduate Studies

UTAH STATE UNIVERSITY
Logan, Utah

2018

ABSTRACT

In Vitro Simulation of Microgravity Induced Muscle Loss Successfully Increases Expression of Key In Vivo Atrophy Markers

by

Charles P. Harding, Master of Science

Utah State University, 2018

Major Professor: Dr. Elizabeth Vargis
Department: Biological Engineering

Muscular atrophy, defined as the loss of muscle tissue, is a serious issue for immobilized patients on Earth and in human spaceflight, where microgravity prevents normal muscle loading. *In vitro* modeling is an important step in understanding atrophy mechanisms and testing countermeasures before animal trials. The most ideal environment for modeling must be empirically determined to best mimic known responses *in vivo*.

To simulate microgravity conditions, murine C2C12 myoblasts were cultured in a rotary cell culture system (RCCS). Alginate encapsulation was compared against polystyrene microcarrier beads as a substrate for culturing these adherent muscle cells. Changes after culture under simulated microgravity were characterized by assessing mRNA expression of MuRF1, MAFbx, Caspase 3, Akt2, mTOR, Ankrd1, and Foxo3. Protein concentration of myosin heavy chain 4 (Myh4) was used as a differentiation marker. Cell morphology and substrate structure were evaluated with brightfield and fluorescent imaging.

Differentiated C2C12 cells encapsulated in alginate had a significant increase in only MuRF1 following simulated microgravity culture and were morphologically dissimilar to normal cultured muscle tissue. On the other hand, C2C12 cells cultured on polystyrene microcarriers had significantly increased expression of MuRF1, Caspase 3, and Foxo3 and easily identifiable multi-nucleated myotubes. The extent of differentiation was higher in simulated microgravity and protein synthesis more active with increased Myh4, Akt2, and mTOR. The *in vitro* microcarrier model described herein significantly increases expression of several of the same atrophy markers as *in vivo* models. However, unlike animal models, MAFbx and Ankrd1 were not significantly increased and the fold change in MuRF1 and Foxo3 was lower than expected.

Using a standard commercially available RCCS, the substrates and culture methods described only partially model changes in mRNAs associated with atrophy in vivo. Nevertheless, our results *in vitro* are highly significant for MuRF1 ($p<0.01$), Foxo3 ($p<0.01$), and Caspase 3 ($p<0.001$), indicating that with further development, simulated microgravity systems may present a promising system for investigation of atrophy pathways and first-step design and selection of novel therapeutics necessary to ensure astronaut health and fitness during long-term spaceflight. (97 pages)

PUBLIC ABSTRACT

In Vitro Simulation of Microgravity Induced Muscle Loss Successfully Increases Expression of Key In Vivo Atrophy Markers

Charles P. Harding

Muscle loss from lack of activity is a serious issue for immobilized patients on Earth and in human spaceflight, where the low gravity environment prevents normal muscle activity. Simulating muscle loss in cultured cells is an important step in understanding how this condition occurs. This work evaluates different means of simulating muscle loss and selects the one that most closely mimics the cellular responses seen in animals and humans.

To simulate the microgravity environment of spaceflight, mouse skeletal muscle cells were grown in a rotary cell culture system (RCCS). Growing the cells within a natural gelled substrate was compared against growing them on the surface of small plastic beads. Changes after culture under simulated microgravity were characterized by assessing proteins and genes known to change during muscle loss. The structure of the cells was also evaluated by microscopy.

The mouse skeletal muscle cells grown on plastic beads in the RCCS had significant changes in multiple key genes associated with muscle loss and demonstrated physical characteristics expected of mature tissue in live animals. This model is a valuable platform for exploring muscle loss mechanisms and testing new drugs.

ACKNOWLEDGMENTS

I thank my advisor, Dr. Elizabeth Vargis, for her guidance, support, and for giving me the freedom to pursue this research. This work was also supported by the Utah NASA Space Grant Consortium (UNSGC) Graduate Fellowship (Harding, C.) and by the US Nuclear Regulatory Commission (NRC-HQ-84-15-G-0033). Within the Vargis lab, I would like to especially thank Cindy Hanson, Farhad Farjood, Lori Caldwell, and Matt Clegg for their detailed feedback on my papers and presentations, as well as their suggestions on my research direction.

I thank Dr. Jon Takemoto for his support in sharing his materials and knowledge about mesobiliverdin and the underlying mechanisms. I thank Dr. Timothy Taylor for introducing me to alginate encapsulation methods and their use in bioreactors.

Finally, I thank my supervisors at GE Healthcare, Joseph Camire, Linda Clade, Gerald (Dusti) McEwen, and Kalle Johnson for their incredible flexibility and sharing their many years of knowledge during the course of my graduate work.

Charles P. Harding

CONTENTS

LIST OF TABLES

Table Page

LIST OF FIGURES

Figure Page

LIST OF ABBREVIATIONS

Ankrd1 – Cardiac ankyrin repeat protein 1

Akt – Protein kinase B

BCA – Bicinchoninic acid

BCAA – Branched-chain amino acid

BSA – Bovine serum albumin

BVR – Biliverdin reductase

C2C12 – Immortalized mouse myoblast cell line

DMEM – Dulbecco's modified eagles medium

DNA – Deoxyribonucleic acid

DPBS – Dulbecco's phosphate buffered saline

E1, E2, E3 – Ubiquitin-conjugating enzyme 1, 2, 3

EDTA – Ethylenediaminetetraacetic acid

FBS – Fetal bovine serum

FOXO3 – Forkhead box O3

GAPDH – Glyceraldehyde 3-phosphate dehydrogenase

H2AX – H2A histone family, member X

HCl – Hydrochloric acid

HEPES – 4-(2-hydroxyethyl)-1-piperazineethanesulfonic acid

HO-1 – Heme oxygenase 1

HPLC – High-performance liquid chromatography

HRP – Horseradish peroxidase

IgG – Immunoglobulin G

MAFbx – Muscle atrophy F-box

mRNA – Messenger ribonucleic acid

mTOR – Mammalian target of rapamycin

MuRF1 – Muscle RING finger-1

Myh4 – Myosin heavy chain 4

MyoD – Myogenic differentiation protein 1

NASA – National Aeronautics and Space Administration

PEO – Poly(ethylene oxide)

PI3K – Phosphatidylinositol-4,5-bisphosphate 3-kinase

PLG – Poly(lactide-co-glycolide)

PTEN – Phosphatase and tensin homolog

PVA – Poly(vinyl alcohol)

PVDF – Polyvinylidene difluoride

qRT-PCR – Quantitative real-time polymerase chain reaction

RBE – Relative biological effectiveness

RCCS – Rotary cell culture system

RIPA – Radioimmunoprecipitation assay

RNA – Ribonucleic acid

ROS – Reactive oxygen species

SDS – Sodium dodecyl sulfate

T25 – Tissue culture flask, 25 cm^2 culture area

T75 – Tissue culture flask, 75 cm^2 culture area

TBST – Tris-buffered saline with tween 20

ULA – Ultra low attachment

CHAPTER 1

INTRODUCTION

Motivation and Scope

Skeletal muscle loses significant strength and mass during extended periods of inactivity, with losses of 40% reported after 6 months in orbit[1]. Not limited to spaceflight, the causes of inactivity also include immobilization of broken limbs, paralysis, and bed rest. Reducing muscle loss associated with inactivity is critical for preserving the strength and endurance of astronauts, especially with future long-term missions planned for Mars. Muscle mass loss for short duration missions ranges from 10-20%, compared to 30-50% for long duration missions[2, 3]. To reduce these risks, flight protocol at the National Aeronautics and Space Administration (NASA) mandates that crew members exercise on missions lasting over 10 days; however, loss of strength and muscle mass has been reported after only 5 days[4, 5]. Earth-bound patients would also benefit from faster recovery times and reduced need for physical therapy following serious injuries. Approximately 40-50% of total body mass is skeletal muscle and its loss can induce numerous detrimental physiological changes, including reduced power, lower endurance, and atypical reflex responses[6, 7]. While many promising anti-atrophy compounds have been identified, testing them in actual spaceflight conditions would be prohibitively expensive and time consuming.

Modeling the atrophy-inducing microgravity environment of space in a ground-based laboratory has several challenges. The multiple animal models of atrophy, including hindlimb unloading, limb casting, tendonectomy, and nerve blocking only

affect a small portion of the body. While localized atrophy effects can be studied using these methods, systemic effects of whole body atrophy, as would be experienced in spaceflight, are not accurately modeled. Localized, tissue-specific atrophy can also be modeled *in vitro* at a significantly lower cost and without the regulatory oversight necessary for animal models. Clinostats and rotary cell culture systems move the cells such that the sum of gravitational vectors over time is approximately zero. However, the growth substrate and culture process must be optimized for the selected cell line to maximize changes in the desired atrophy markers versus the control.

Here, we have developed a ground-based model that mimics microgravity-induced expression of the mRNA atrophy markers MuRF1, MAFbx, and Caspase 3 *in vitro* using a rotary cell culture system and the C2C12 mouse skeletal muscle cell line. This model provides consistent and significant increases in the selected markers and a means of screening anti-atrophy therapeutics prior to testing *in vivo.* Additionally, external radiation can be applied to the system to more accurately mimic the spaceflight environment. We expect the model will be valuable for probing atrophy mechanisms and expediting the search for pharmaceuticals that enable long-duration spaceflight missions and improve patient outlook.

Organization

This thesis describes development of a model for mimicking atrophy of skeletal muscle cells *in vitro*, including growth substrate selection, application of low-dose radiation, and metrics for morphology, gas transfer, amino acids, metabolites, proteins,

and mRNAs. Chapter 2 provides a background on the mechanisms of spaceflight atrophy and a literature review of atrophy modeling *in vivo* and *in vitro*. Additionally, it highlights where the model developed herein fits into the current body of literature.

Chapter 3 details the preliminary work in developing the microgravity model. Selection of an appropriate control vessel, growth substrate, and culture methodology is discussed. Use of amino acid and metabolite analysis for distinguishing between normal gravity controls and simulated microgravity conditions is evaluated. Finally, addition of low-dose gamma radiation is investigated.

Chapter 4 is a manuscript prepared for the Utah NASA Space Grant Consortium. Chapter 5 contains the final model and metrics developed in this thesis, as will be submitted for publication. Chapter 6 summarizes the main findings of this thesis and concludes with future work involving anti-atrophy compounds, higher-dose radiation, and additional cell lines.

CHAPTER 2

BACKGROUND AND LITERATURE REVIEW

Mechanisms of spaceflight atrophy

Astronauts experience significant muscle loss in spaceflight despite the current International Space Station exercise program[8]. Disuse, reduced protein synthesis, and reduced motor neuron activity all contribute to loss of muscle tissue and strength in spaceflight[6]. The degree of atrophy is dependent on anatomical region and duration of exposure to the microgravity environment. Short duration missions can result in a 10-20% loss of muscle mass, where losses in long duration missions can range from 30-50%[2, 3]. Atrophy is more severe for muscles responsible for maintaining posture under normal gravity, with the intrinsic back muscles losing 10.3% volume compared to 3.9% for calf muscles after 8 days of spaceflight[2, 9]. Atrophy affects cardiac muscle in addition to skeletal muscle, with a decrease in left ventricular mass of 12% following 10 days of spaceflight[10]. Preventing muscle atrophy would preserve the strength and endurance of astronauts and help enable longer duration space travel and exploration.

The mRNA atrophy markers MuRF1, MAFbx, and Caspase 3 are all critical components of muscle tissue breakdown via the ubiquitin proteasome pathway. In this pathway, ubiquitin—a polypeptide co-factor—attaches to the protein to be degraded, the complex is recognized by the 26S proteasome, then broken down into its constituent amino acids[11]. There are three enzymes involved in attaching ubiquitin to the protein, E1, E2, and E3. The E3 ubiquitin ligases are the most diverse group, with up to 1000 different ligases serving this role in mammals[11]. Two key E3 ubiquitin ligases involved

in attaching ubiquitin to proteins are MuRF1 and MAFbx, both upregulated in a wide range of atrophy models including denervation, hindlimb unloading, immobilization, bed rest, multiple diseases, spaceflight, and aging[12, 13]. MAFbx and MuRF1 aren't upregulated for all types of atrophy. Contrary to atrophy from immobilization, sarcopenia, or age-related muscle loss, results in a down-regulation of these key ubiquitin ligases, indicating that multiple mechanisms need to be investigated for a total picture of muscle loss[14]. This thesis focuses on loss from a simulated microgravity environment.

The role of the third mRNA marker, Caspase 3, comes into play in the first stages of atrophy. Intact muscle fibers can't be degraded by the ubiquitin proteasome system and must be broken down before MuRF1 and MAFbx can act. Reactive oxygen species—increased during muscular atrophy—upregulate calpains, which degrade multiple muscle-related proteins, including titin, nebulin, actin, and myosin[7]. Reactive oxygen species (ROS) also increase Caspase 3, which breaks down actomyosin complexes in the muscle tissue[7, 11]. Treatment with vitamin-E, a potent antioxidant, significantly reduced Caspase 3 expression in mice subject to 14 days unloading, but did not bring the expression level all the way down to the control[15]. A cell culture model that successfully mimics *in vivo* atrophy should demonstrate upregulation of Caspase 3 for the initial stages of muscle breakdown, as well as MuRF1 and MAFbx for the later stages of protein recycling via the ubiquitin proteasome system.

Blocking the ubiquitin proteasome system can have therapeutic effects, but is not a feasible method for attenuating atrophy. Antigenic peptides produced following protein degradation are presented to lymphocytes, which then produce antibodies[11]. One such proteasome inhibitor, Bortezomib, is an effective chemotherapeutic agent, but also acts as

an immunosuppressant[16]. Likewise, blocking Caspase 3 to prevent muscle atrophy is not a viable solution. Caspase 3 inhibited C2C12 cells and primary myoblasts from Caspase 3 null mice displayed markedly reduced differentiation[17].

In addition to upregulating Caspase 3, ROS play an additional role in muscle atrophy via degradation of muscle fibers[18]. As astronauts travel past the protection of the Earth's magnetic field, they experience increased radiation levels which generate ROS by the radiolysis of water[19]. Even after returning to Earth, ROS generated by microgravity and irradiation can continue to disrupt cellular systems. Harmful radiation in space primarily comes in two forms, gamma rays and high energy heavy ions[20]. Radiation intensity fluctuates depending on solar activity and proximity to the Earth. The lowest radiation dose rates occur when in close proximity to the Earth and during the solar maximum[20]. Gamma rays are a form of electromagnetic radiation with no mass while high energy heavy ions are atomic nuclei stripped of electrons and moving at relativistic velocities. Some high energy heavy ions are produced by the Sun, but most come from distant supernovae.

Relative biological effectiveness (RBE) is a measure of how damaging a particular type of radiation is to living tissue. Gamma radiation is assigned an RBE of 1 by definition. High energy heavy ions can have RBE values ranging from 20-40, indicating significantly more tissue damage for an equivalent dose[21]. Although high energy heavy ions present a greater health hazard in spaceflight, they are difficult to simulate in a laboratory and require large particle accelerators to produce. In contrast, gamma radiation sources are relatively inexpensive and a large body of data exists

regarding epidemiological studies in radiation-exposed humans, rodents, and non-human primates.

NASA limits astronaut radiation exposure to levels that correspond with a 3% increase in fatal cancer risk[22]. Long-term missions beyond low Earth orbit, such as a journey to Mars, exceed this limit within a single mission and increase the risk of developing cancer[20]. Due to the highly penetrating nature of high energy ions in cosmic radiation, shielding the spacecraft is not economically feasible[20]. Biological countermeasures to radiation damage and increased cancer risk provide an attractive alternative to heavy and costly shielding.

One cellular response that counters radiation damage is the up-regulation of heme oxygenase-1 (HO-1)[23, 24]. HO-1 is induced in response to oxidative stress and combats this stress in part by degrading heme into biliverdin-IXα, a natural antioxidant and anti-inflammatory[25]. Artificial induction of HO-1 has demonstrated protective effects against ionizing radiation in multiple tissue types[24, 26]. Another promising atrophy and radiation countermeasure is vitamin E. The antioxidant effects of vitamin E scavenge free radicals and reduce expression of calpains and Caspase 3, -9, and -12, reducing muscular atrophy due to immobilization and unloading[27, 28]. In addition to preventing muscle loss, vitamin E also preserves bone mass and strength following unloading[29]. Several forms of vitamin E have demonstrated radioprotective effects, including α-tocopherol, δ-tocotrienol, and γ-tocotrienol[30–32].

In summary, muscular atrophy is a complex process involving multiple pathways interlinked with other critical cellular functions. Understanding how modifying one pathway might influence other systems is vital in development of therapeutics. *In vitro*

modeling, as described in this thesis, is well suited to evaluating changes in cell metabolism and mRNA expression induced by experimental drugs.

Atrophy modeling in vivo

A classic method for simulating weightlessness is the hind limb unloading rodent model, developed at NASA in the 1970's[33]. In this model, the rodent is affixed in a harness or tail traction device such that the hind limbs are elevated at a 30° angle[33]. The resulting unloading induces differential muscle atrophy in the hind limbs and cephalic fluid shift similar to real microgravity conditions[33]. Three commonly measured mRNAs in muscle loss modeling are muscle RING finger-1 (MuRF1), muscle atrophy F-box (MAFbx), and Caspase 3, all upregulated in numerous rodent models of muscular atrophy including disease, immobilization, hind limb unloading, as well as spaceflight[12, 15, 34–45]. Following hind limb unloading, knockout mice lacking MuRF1 and MAFbx display significantly less atrophy than wild type mice, highlighting the importance of those ligases in the mechanisms underlying muscle loss[12, 35].

Cages for hindlimb unloading must be designed to accommodate the specific requirements of each experiment. Metabolism can be monitored by attaching a specially designed urine and feces separator to the bottom of the cage[46]. If radiation will also be administered, the animal must either be moved to a smaller container that restricts movement, thereby ensuring the dose is consistent and localized, or a lower dose radiation source must be attached to the cage itself[47, 48]. A lower activity radiation source, such as a cobalt 57 plate under the cage, can provide a whole-body dose for the

duration of the experiment. This constant, lower level dose is more similar to spaceflight than periodic acute doses. However, if additional types of radiation, such a proton or heavy ion, are desired, the animals must be moved to a synchrotron or particle accelerator and an acute dose administered.

Animal models have the benefit of providing a variety of tissue types following completion of microgravity simulation and irradiation. In addition to muscle tissue, hindlimb unloading and irradiation studies have investigated bone, cardiovascular function, immunology, renal function, neurology, reproductive systems, and oxidative stress[49–53].

In conclusion, animal models using hindlimb unloading and other immobilization methods are a common and effective means of simulating multiple changes, including atrophy from the microgravity environment. However, ground-based animal models are more time consuming, more expensive, and are subject to more regulation than cell culture models, providing strong motivation to develop other methods. Newly developed therapeutics can be effectively screened with smaller quantities in cell culture models and safe dose ranges established prior to testing *in vivo*.

Atrophy modeling in vitro

In vitro simulation of microgravity can be conducted with rotary culture systems and 3D random positioning machines or clinostats[54, 55]. *In vitro* microgravity simulation has the benefits of lower costs and fewer regulatory concerns compared to animal models. For use in drug development, the quantity of test compound required to

elicit a response is lower for small *in vitro* systems, conserving therapeutics that may be difficult to produce at early stages of development.

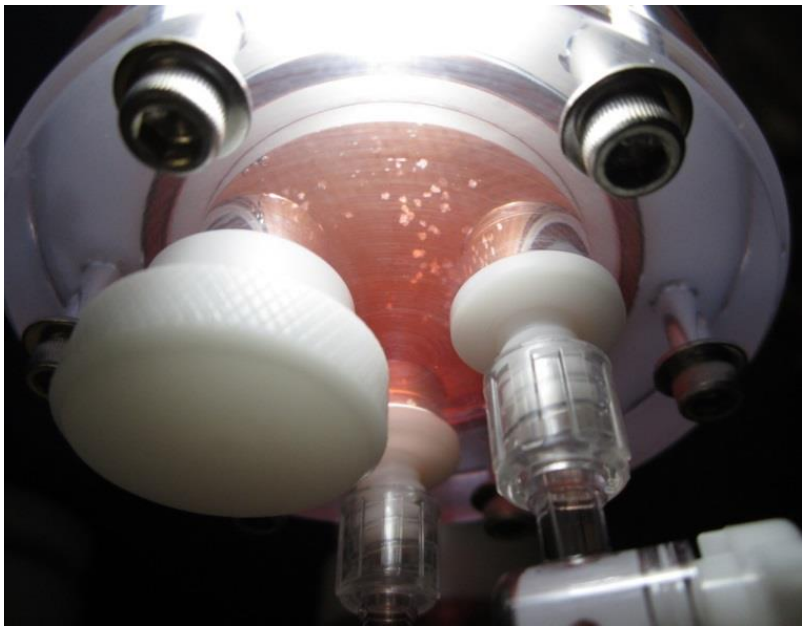

Figure 1. Microcarrier clusters with C2C12 cells suspended in the RCCS.

Atrophic conditions can be generated in ground-based laboratories with a rotary cell culture system (RCCS), developed by Synthecon Inc. in conjunction with NASA to simulate microgravity[54]. Microgravity is simulated by the rotational motion of the vessel maintaining cells at their terminal settling velocity, similar to what astronauts experience in orbit around Earth [Figure 1]. Fluid flow in the RCCS had been designed to provide a low shear environment[54]. The settling velocity is described by the equation $v_s = \frac{2g(\rho_a - \rho)R_a^2}{9\mu}$, where ρ_a is the density of the cell aggregate, ρ is the density of the culture media, R_a is the radius of the cell aggregate, and μ is the fluid viscosity[56].

When the substrates are maintained at their terminal settling velocity, the force of gravity F_g is described by Stoke's Law.

$$F_g = (\rho_a - \rho) g \frac{4}{3} \pi R^3$$

The resulting F_g is balanced by the drag force from the rotating fluid, resulting in a net force of zero. Since g and R are constant at any given moment, the ratio of F_g in the RCCS to the normal force of gravity can be simplified to express how many times normal gravity (Xg) is produced within the system.

$$Xg = \frac{F_{g\ RCCS}}{F_{g\ Normal}} = \frac{(\rho_a - \rho) g \frac{4}{3} \pi R^3}{m \times a} = \frac{(\rho_a - \rho) g \frac{4}{3} \pi R^3}{(\rho_a \times \frac{4}{3} \pi R^3) g} = \frac{\rho_a - \rho}{\rho_a}$$

As a result, the final force of gravity on the cells is dependent entirely on the density of the substrate and surrounding fluid. To minimize the force of gravity, a cell culture substrate with a density close to that of water should be selected.

The RCCS has been used to simulate microgravity in a variety of cell types, including lymphocytes, osteoblasts, and myoblasts[57–59]. The C2C12 cell line used in the experiment presented herein is a mouse myoblast line that can differentiate into contractile skeletal muscle fibers. The cells can be tested in their undifferentiated state to investigate effects on developing tissue, as well as in their differentiated state to investigate effects on mature tissue. First cultured in 1977, the C2C12 cell line produces many of the same proteins and mRNAs as human muscle tissue, making it a suitable analog for investigation of atrophic conditions[60].

As an adherent cell line, C2C12 cells require a substrate for growth. A three-dimensional scaffold suitable for culture of adherent cell lines such as C2C12's can be formed from a wide variety of synthetic and naturally occurring hydrogels[61]. Selection

of a scaffold should include considerations for compatibility with the desired cell type, physical characteristics, diffusion rate, and ease of gelling and dissolution. Scaffolds such as poly(lactide-co-glycolide) (PLG) have good mechanical properties and excellent biocompatibility for use in vivo, but harsh processing conditions makes encapsulation of viable cells challenging[61]. Other synthetic polymers such as poly(ethylene oxide) (PEO) and poly(vinyl alcohol) (PVA) have established medical applications for tissue engineering and drug delivery, but photo-crosslinking of PEO with UV light and PVA with repeated freeze-thaw cycles or glutaraldehyde would damage encapsulated cells[61]. In contrast, the naturally occurring hydrogel alginate has well established uses for cell encapsulation due to low toxicity and gentle gelling conditions[61–66]. The high porosity of alginate hydrogels is advantageous for maximizing diffusion rates and ensuring adequate exchange of nutrients and waste products with the surrounding culture media[62]. Dissolution of alginate hydrogels for cell harvesting can be accomplished with a neutral buffered solution of sodium citrate.

Encapsulation of mammalian cells in alginate hydrogels to generate 3D cultures has been performed on many cell types, including stromal vascular cells, Leydig cells, baby hamster kidney cells, epithelial cells, fibroblasts, and myoblasts[63–66]. Diffusion of nutrients through the alginate bead is a function of molecule size and the percentage of alginate, with smaller molecules and lower alginate percentages resulting in faster diffusion[67]. The percentage alginate used for encapsulation can be varied between 1.5-3% (w/v) depending on the cell type and desired mechanical properties[63–66, 68]. To preserve bead integrity in the dynamic RCCS environment, we elected to encapsulate cells at the upper end of the range to maximize mechanical strength of the beads [Figure

2][62]. Mechanical stability of alginate beads can also be modified by complexing with chitosan[63]. Additionally, alginate beads can be formed in various sizes by changing the gauge of the needle used for extrusion. In contrast with microcarrier beads, which are limited to seeding with undifferentiated cells, alginate encapsulation can be performed on both undifferentiated and differentiated muscle cells. The tunable properties and low cost of alginate hydrogels make them an attractive substrate for 3D cultures.

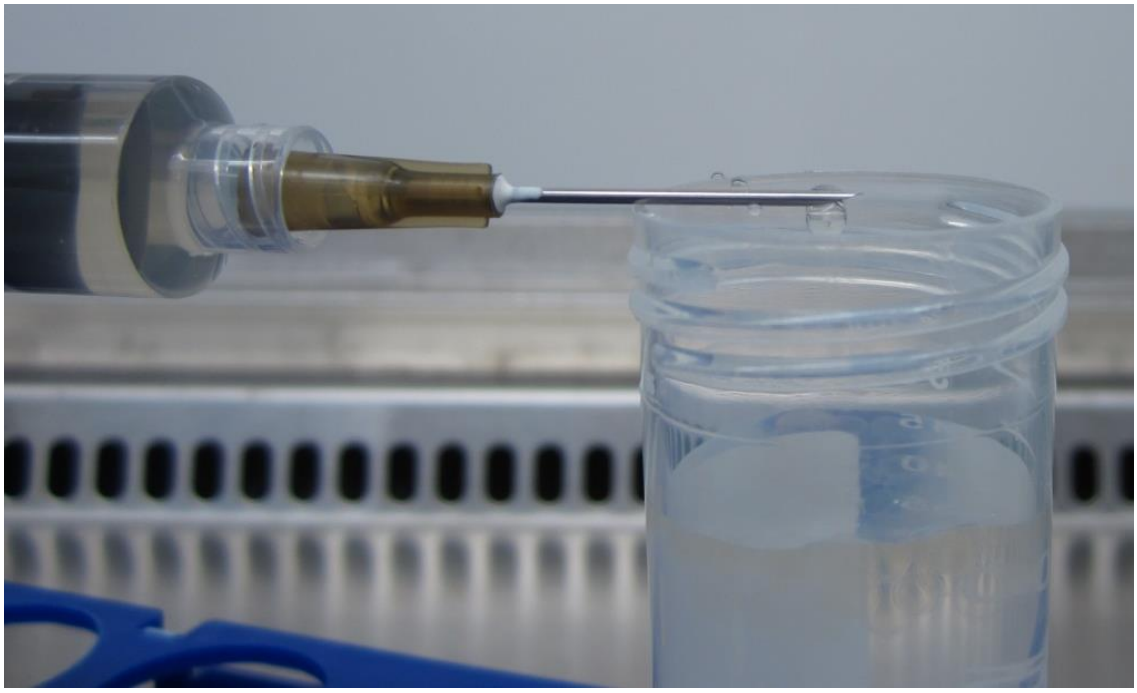

Figure 2. C2C12 cells suspended in 3% w/v alginate solidifying in 200 mM $CaCl_2$, 10mM HEPES

Another option for culturing adherent cells in the suspension environment of the RCCS is microcarriers, small synthetic beads with a suitable surface chemistry [Figure 3]. The ease of scalability makes microcarriers an attractive substrate for producing large quantities of cells for therapeutic applications[69, 70]. A wide variety of surface

chemistries are available from suppliers to tailor the beads for specific cell types and culture conditions[69]. Successful culture of muscle cells on microcarriers has been reported with dextran, collagen, and polystyrene surfaces[56, 71, 72]. While a more expensive substrate than alginate, the variety of commercially available bead types, ease of use and facile scalability make microcarriers an industry standard for suspension culture of adherent cells.

Figure 3. HyQ Sphere Pplus 102-L Polystyrene microcarriers

Conclusion

Previously published work with muscle cells, including C2C12s, in simulated microgravity focused on changes in differentiation induced by culture in the RCCS[56,

59, 73]. To the best of the authors' knowledge, no previously published work has investigated changes in atrophy-specific mRNAs with muscle cell culture in the RCCS. The work presented in this thesis combines the mRNA analytics of *in vivo* atrophy modeling with the *in vitro* RCCS, supporting use of cultured muscle cells in investigations of atrophic mechanisms.

CHAPTER 3

PRELIMINARY WORK

Overview

This section covers selection of the control cell culture vessels and alginate encapsulation conditions used in Chapters 4 and 5. Additionally, metrics for distinguishing between control and simulated microgravity conditions are discussed. We initially sought to use analysis of cell metabolites and amino acids to determine culture status. However, these methods did not have sufficient resolution to distinguish between conditions. Nevertheless, key results of branch chain amino acid levels and glucose consumption are presented to demonstrate typical concentrations under simulated microgravity conditions.

Selection of static control vessel for microcarriers

A control vessel in a simulated microgravity cell culture model should meet three criteria: same volume as RCCS vessels, suitable surface chemistry, and single gravitational vector. An identical media volume is needed to control for the quantity of nutrients available to the cells. A low adhesion surface chemistry in the control vessel is critical in microcarrier cultures to force cells to grow only on the microcarrier beads. Use of a cell culture treated flask with microcarriers provides a larger surface area for growth than would be available in the RCCS and results in microcarriers stuck to the surface of the flask. Finally, the control vessel should either be static or agitated in a manner that

results in a single primary gravitational vector, such as an orbital shaker at low speed or rocker plate.

Two vessel types were evaluated for culture of microcarriers as a normal-gravity control, the Nunc OptiCell cartridge and the Corning ultra-low attachment flask [Figure 4]. Both vessels have a 10 mL working volume, equivalent to that of the vessels used with the RCCS. The OptiCell cartridge has the advantage of a gas-permeable membrane with a high surface area to volume ratio, resulting in increased oxygen saturation during the earlier stages of the culture [Figure 5]. However, the cartridge requires all fluid handling be done through a syringe needle, which is easily clogged by the microcarrier beads. Due to the clogging, added expense of using syringes instead of pipette tips, and dissimilar dissolved oxygen profile compares to the RCCS, T25 flasks with an ultra-low attachment surface were selected as the normal gravity control vessels.

Initially, the control flasks were cultured on a rocker plate to account for fluid motion in the RCCS. However, the rocker plate forced all the microcarrier beads into a single large mass not representative of the cluster sizes in the RCCS. A low speed orbital shaker produced a similar result. When properly filled and absent of air bubbles, shear forces from fluid motion in the RCCS are negligible and selecting a control with similar bead cluster morphology is preferred[54]. Therefore, static ultra-low attachment flasks were selected as the optimum control.

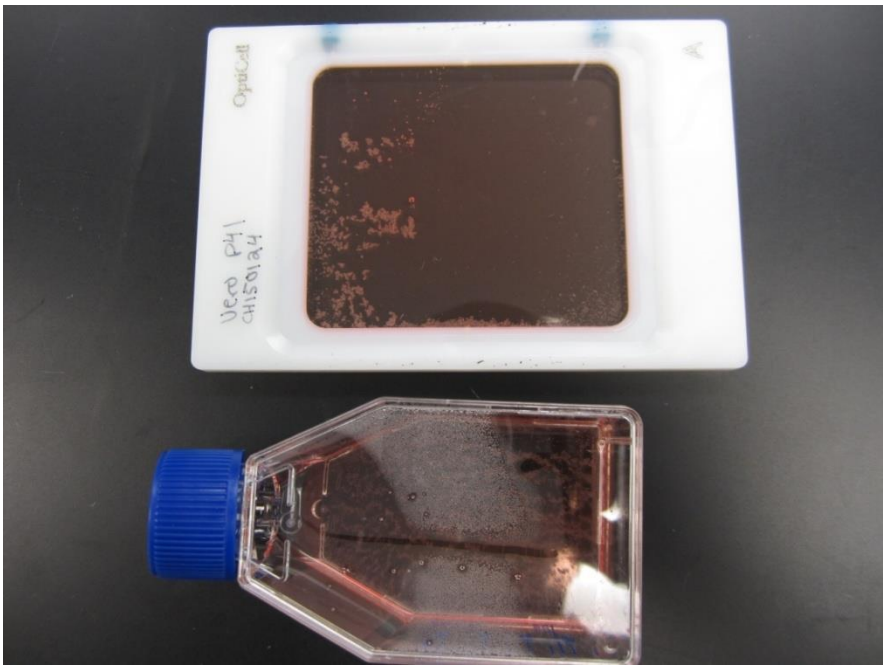

Figure 4. OptiCell cartridge (top) compared to a standard T25 (bottom) for static normal-gravity controls.

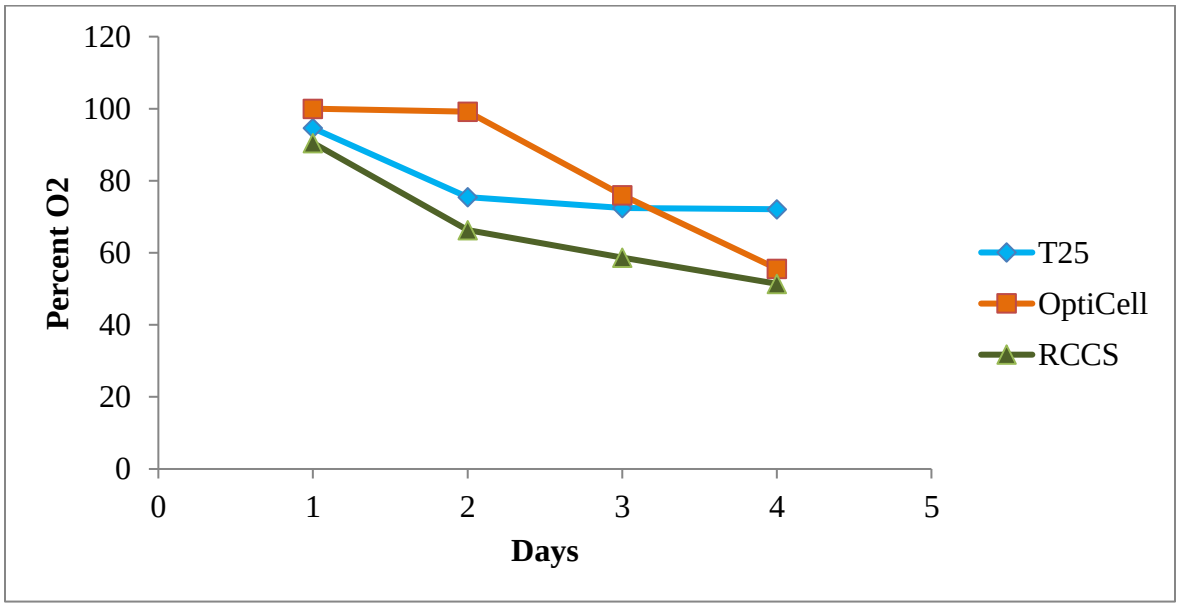

Figure 5. Oxygen saturation of cell culture media in each vessel, n=1.

Optimization of encapsulation conditions

Encapsulating and immobilizing cells within an alginate hydrogel is another means of generating a 3D cell mass. Unlike microcarriers, where monolayers of cells freely grow on the surface of the substrate, alginate encapsulation locks cells in place within the substrate. The conditions under which cells are encapsulated, including cell density, alginate percentage, and the use of additives such as chitosan can all influence the culture performance. This section discusses the steps taken to determine the encapsulation parameters best suited for use with the RCCS.

The cell density for encapsulation was selected to maximize cell-cell contact within the alginate bead while maintaining bead integrity. It was observed that cells have difficulty spreading through the bead, likely due to the high density of the 3% w/v alginate substrate. While the percentage alginate used for encapsulation can be varied between 1.5-3% (w/v), we elected to encapsulate cells at the upper end of this range to maximize mechanical strength of the beads in the dynamic RCSC environment[62–66, 68].

To limit the distance the cells needed to spread before contacting another cell, seeding density optimization was performed. Undifferentiated cells were encapsulated at densities of 0.25, 0.5, 1, and $10x10^6$ cells/mL alginate. Differentiated cells were encapsulated following 10 days of culture in standard tissue culture flasks, after which there were removed with a cell scraper and encapsulated at 75 or 150 cm^2 of flask area per mL of alginate.

A syringe pump with a multi-syringe head was used to form alginate beads at multiple encapsulation densities simultaneously [Figure 6]. With a 19 gauge needle and a flow rate of 2 mL/min, the average bead size was 3251±103 µm, n=10. The size of the beads formed with this method is too large to be aspirated with a serological pipette, requiring the beads to be poured into their culture containers. Use of smaller needles was attempted, but the high cell density resulted in frequent clogging, especially with differentiated cells.

Figure 6. Syringe pump setup for formation of multiple cell-alginate ratio beads.

With undifferentiated cells, the appearance of the beads under brightfield imaging became darker as encapsulation density increased [Figure 7]. Even at the upper end

concentration of $10x10^6$ cells/mL, bead shape was highly spherical. The highest cell density also affords the greatest chance of cell-cell contact necessary for differentiation into multi-nucleated myotubes.

With differentiated cells, at a density of 75 cm^2/mL the beads were mostly full of tissue and still maintained circularity [Figure 8]. At a higher density of 150 cm^2/mL, the beads did not harden into spherical shapes and some droplets broke apart on contact with the $CaCl_2$ solidification buffer [Figure 9]. Therefore, 75 cm^2 of flask area per milliliter of alginate was selected as the ratio for encapsulation of differentiated cells.

The standard alginate croslinking process solidifies the hydrogel, but the beads remain fragile and may be damaged by mechanical forces in the RCCS. Use of chitosan to coat the beads was investigated as a means of improving mechanical durability. Confluent and differentiated C2C12 cells were scraped and encapsulated in alginate beads at a density of 75cm^2/mL alginate. Alginate beads were solidified both with and without cells in either a 0.2 M $CaCl_2$ solution or a 0.5% chitosan solution with 13 mM HEPES and 1.5% (0.135 M) $CaCl_2$[63]. 30 alginate beads were created for each condition. The media was DMEM 10% FBS and was not changed over the duration of the experiment. After 15 days, the beads were removed from the RCCS vessels and imaged. The –Cells +Chitosan vessel had 28/30 beads still present. All other conditions had all 30 beads intact. Significant debris was observed in the +Cells +Chitosan condition [Figure 10 B]. The debris was not present in the +Cells –Chitosan condition [Figure 10 A]. No significant difference was observed in the condition of the beads themselves, but the presence of debris and loss of two beads suggests that 0.5% chitosan may negatively affect bead durability. Chitosan was not used in subsequent experiments.

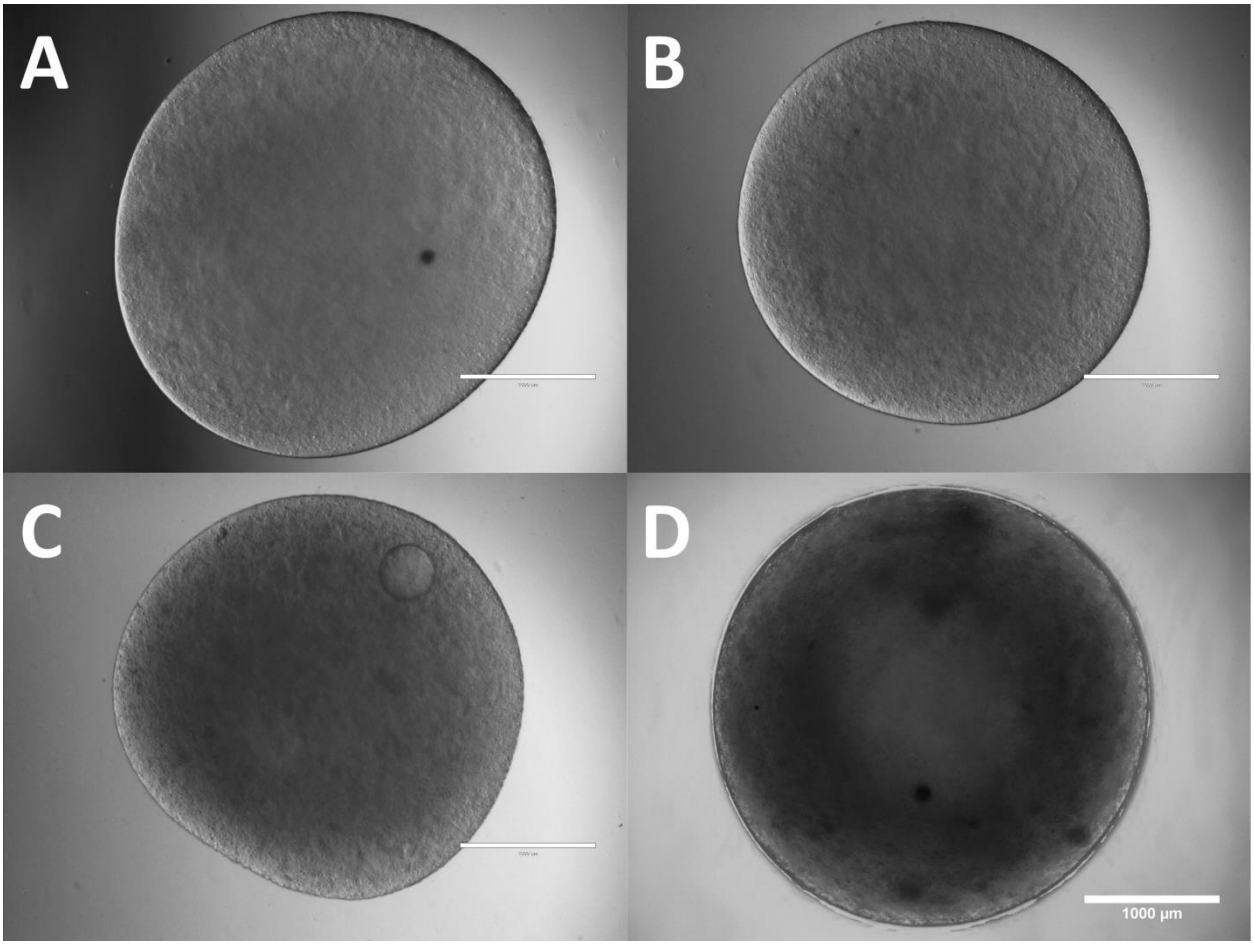

Figure 7. Encapsulation of undifferentiated C2C12 cells at 0.25 (A), 0.5 (B), 1 (C), and 10 (D) x10^6 cells/mL alginate. Scale bar = 1000 µm.

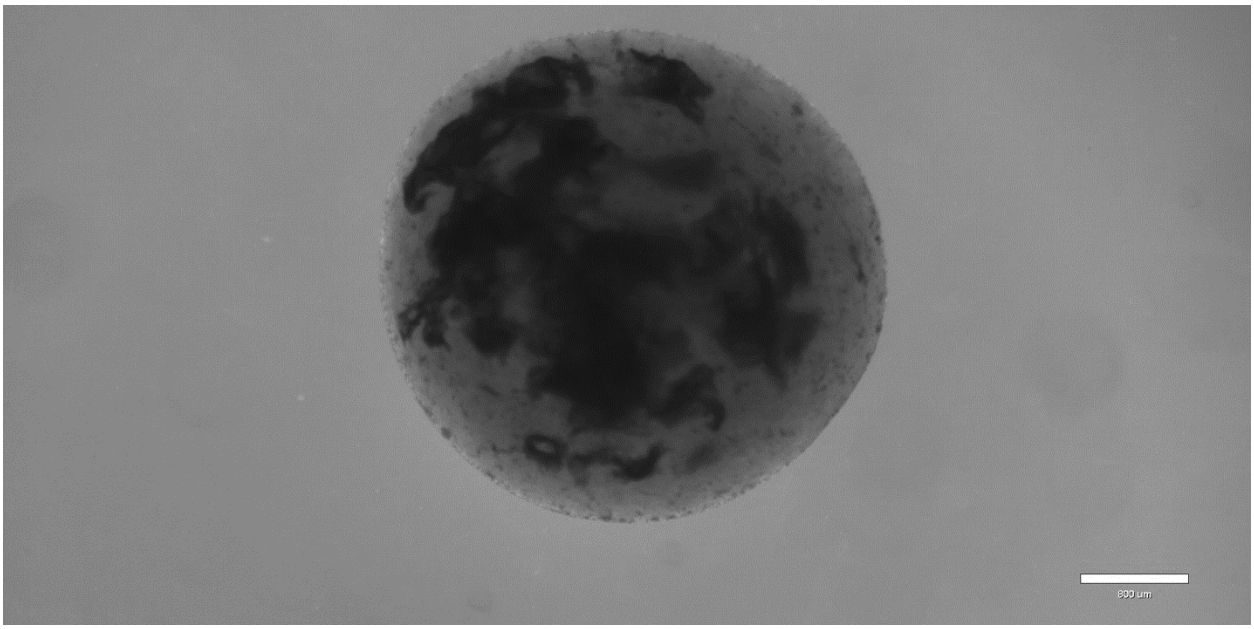

Figure 8. Differentiated cells encapsulated at 75 cm^2/mL alginate

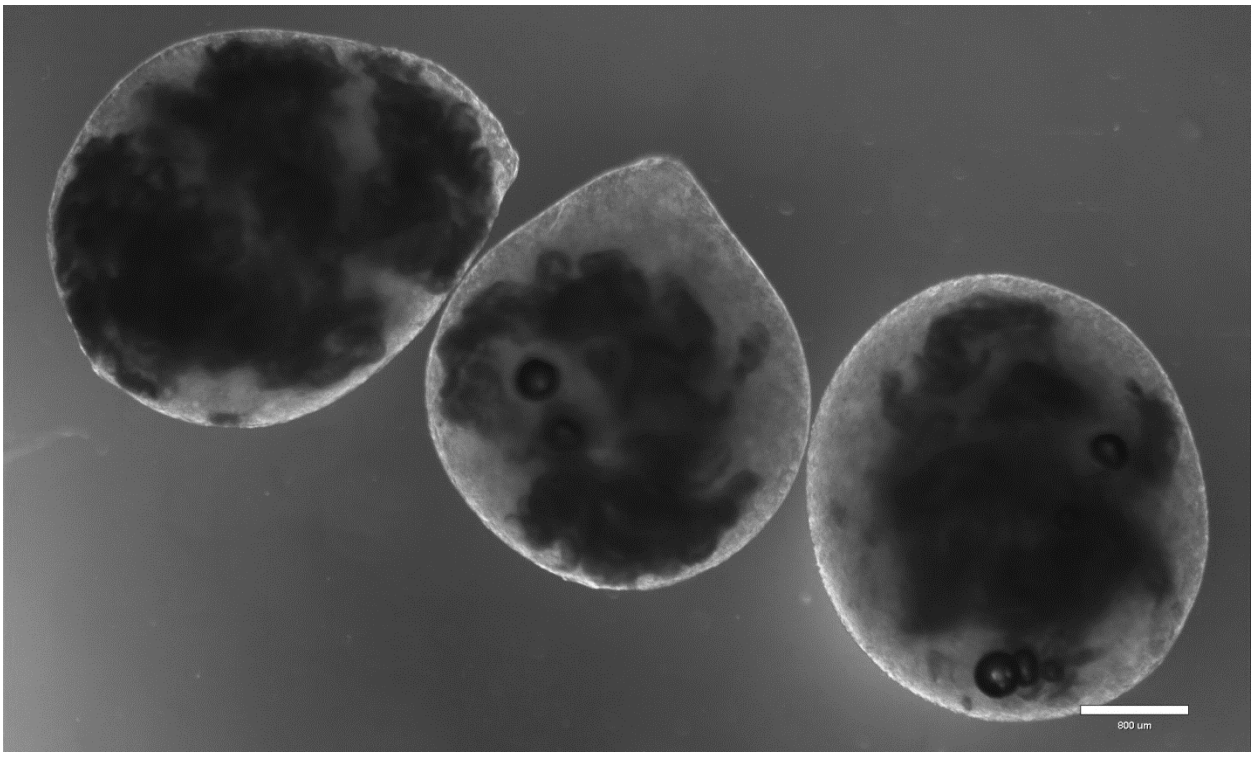

Figure 9. Differentiated cells encapsulated at 150 cm^2/mL alginate

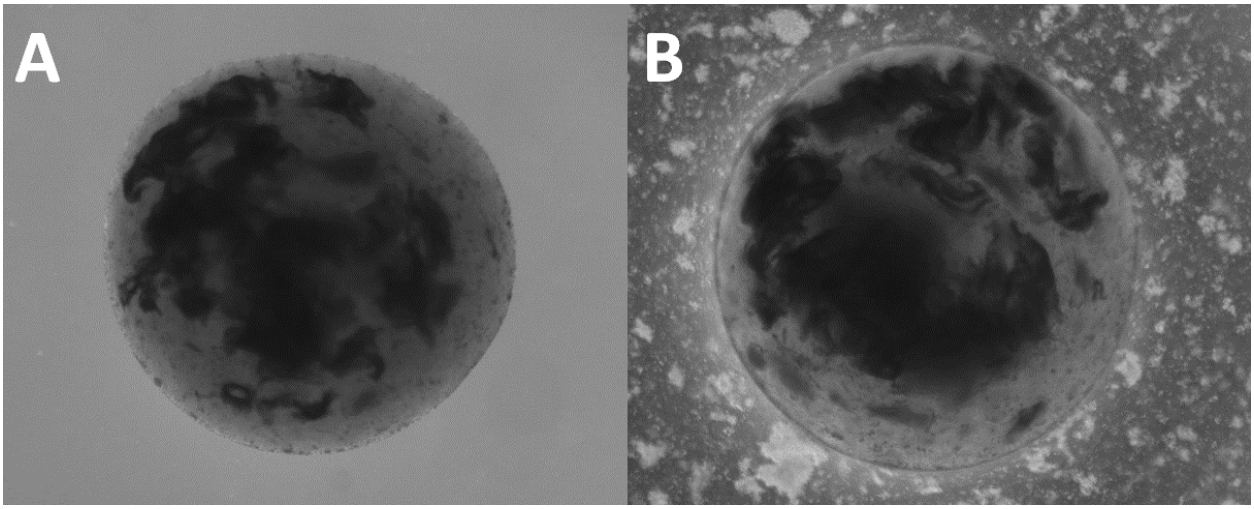

Figure 10. Encapsulated differentiated cells after 15 days of culture in beads without (A) and with (B) chitosan.

Amino acid and glucose analysis

Amino acid concentrations in cell culture media can provide insight into cell metabolism and pathways affected by the experimental conditions. The cell culture process requires a media exchange every 3 days, so data on nutrient consumption is limited to that same timeframe. Preliminary investigation of amino acid levels was performed on day 9 to allow sufficient time for differentiation. A Waters Alliance 2695 high performance liquid chromatography (HPLC) system was used to analyze alanine and the branch chain amino acids (BCAAs) leucine, isoleucine, and valine. Alanine, not present in DMEM, is secreted into the bloodstream by muscle fibers while BCAAs are oxidized for nutrients[74, 75]. Lower alanine production and BCAA consumption would indicate decreased metabolic activity, expected in simulated microgravity.

Alanine was produced by the cells in both experimental conditions, but less was produced in the simulated microgravity condition [Figure 11]. After 9 days, BCAA concentrations were lower in the normal gravity control, indicating higher cell metabolism compared to the simulated microgravity condition. [Figure 11]. Due to small differences between the simulated microgravity condition and DMEM, as well as the regular changing of media introducing variability to the system, HPLC was not used in the following chapters. Instead, qRT-PCR was selected to maximize sensitivity and focus on atrophy markers supported by a large body of literature.

Metabolic activity of the cells was also investigated by measuring glucose consumption with a Nova Biomedical BioProfile FLEX. A decrease in consumption would indicate attenuated metabolism. Glucose consumption decreased sharply between days 6 and 9 for alginate encapsulated cells, while increasing for cells cultured on microcarriers [Figure 12]. Conversely, glucose consumption increased during this period for the microcarrier condition, indicating a higher metabolic rate and more cell growth. The consumption trends are similar for each substrate's respective normal gravity and simulated microgravity conditions [Figure 12].

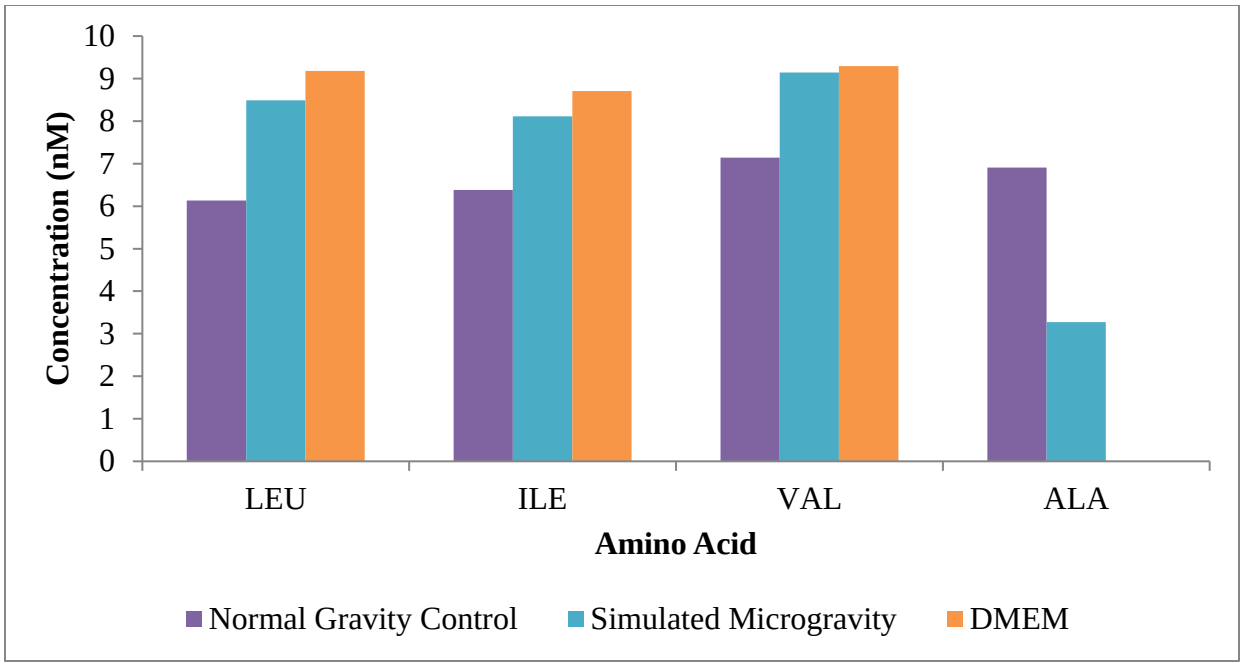

Figure 11. Amino acid levels post-differentiation on day 9. Alanine not present in DMEM.

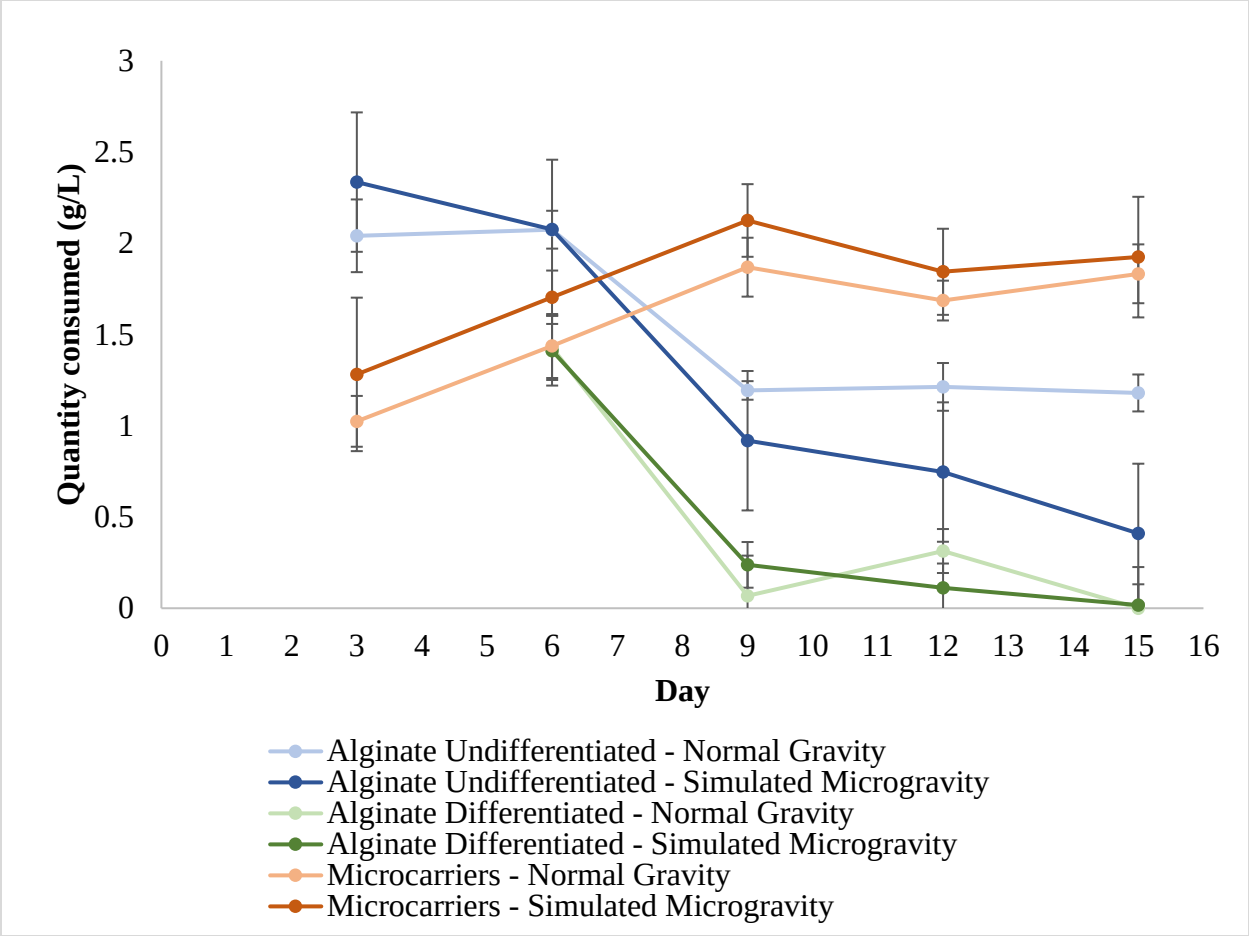

Figure 12. Glucose consumption, as measured by the difference between spent media and fresh DMEM (n=4, error bars are standard deviation).

Conclusion

With amino acid results potentially affected by variations in residual media volume during periodic media changes and similar glucose consumption profiles between RCCS and control conditions, highly sensitive qRT-PCR was selected as the preferred metric for use in Chapter 5. For microcarriers, ultra-low attachment flasks were selected over the OptiCell cartridge; the oxygen profile was similar to the RCCS and bead clusters

were not damaged during liquid handling. The optimized encapsulation density of $10x10^6$ cells/mL and 75 cm^2/mL of alginate was used for subsequent work with undifferentiated and differentiated cells, respectively. Chitosan was not necessary for the mechanical stability of the alginate beads, as 100% of beads without alginate were still intact after the 15-day culture period. With the culture parameters established in this chapter and qRT-PCR identified as a necessary metric, subsequent work in Chapter 5 focused on comparing microcarriers with alginate encapsulation.

CHAPTER 4

UTAH NASA SPACE GRANT CONSORTIUM PAPER

In Vitro Modeling of Microgravity-Induced Muscle Atrophy and Spaceflight Radiation

Abstract

Muscular atrophy, defined as the loss of muscle tissue, is a serious issue for immobilized patients on Earth and in human spaceflight, where microgravity prevents normal muscle loading. A major factor in muscular atrophy is oxidative stress, which is amplified not only by muscle disuse, but also by the increased levels of ionizing radiation in spaceflight. Additionally, elevated radiation exposure can damage DNA, increasing cancer risk.

To model oxidative stress and DNA damage generated by conditions on the International Space Station, murine C2C12 myoblasts were cultured in a rotary cell culture system irradiated by cesium-137. Changes due to the spaceflight model were characterized with fluorescent imaging, amino acid analysis, and enzyme linked immunosorbent assay for heme oxygenase 1. Fluorescent imaging was performed to assess viability, lipid peroxidation, and DNA damage.

Minor DNA damage was observed in cells exposed to 20 μCi cesium-137 for 15 days. No significant differences in viability or lipid peroxidation were noted. Exposure to radiation decreased intracellular heme oxygenase 1 and extracellular alanine, but did not affect branch chain amino acids. Investigation of stronger radiation sources and extended culture time is ongoing. We anticipate that radiation will exacerbate the atrophic effects of microgravity on muscle cells. Simulation of microgravity and spaceflight radiation will

provide a valuable platform for drug discovery and an understanding of the progression from normal to disease state.

Introduction

Muscular atrophy due to disuse is a serious issue for individuals subject to bed rest or prolonged immobilization, as well as in human spaceflight, where microgravity prevents normal muscle loading. Atrophy affects cardiac muscle in addition to skeletal muscle, with a decrease in left ventricular mass of 8% and 12% following 6 weeks of bed rest and 10 days of spaceflight, respectively[10]. Preventing cardiac and skeletal muscle atrophy would preserve the strength and endurance of patients subject to extended bed rest and immobilized limbs, as well as enable longer duration space travel and exploration.

A major factor in muscular atrophy is increased oxidative stress, where reactive oxygen species (ROS) induce degradation of muscle fibers[18]. As astronauts travel past the protection of the Earth's magnetic field, they experience increased radiation levels which generate ROS by the radiolysis of water[19]. Even after returning to Earth, ROS generated by microgravity and irradiation can continue to disrupt cellular systems.

Developing countermeasures for atrophy and radiation in spaceflight will require extensive screening of promising pharmaceuticals for efficacy, safety, contraindications, and dosage schedule. Due to the cost of spaceflight and limited crew time aboard the International Space Station, high throughput screening of pharmaceuticals in actual microgravity conditions is not economically feasible. We propose a ground-based model, detailed herein, to mimic both microgravity and radiation and provide a low cost platform for drug discovery and testing. Anti-atrophy treatments will not only help immobilized

patients on Earth, but will also be critical for future spaceflight missions beyond low Earth orbit.

Background

Atrophic conditions can be generated in ground-based laboratories with a rotary cell culture system (RCCS), developed by Synthecon Inc. in conjunction with NASA to simulate microgravity[54]. Microgravity is simulated by the rotational motion of the vessel maintaining cells in a constant state of free fall, similar to what astronauts experience in orbit around Earth. The RCCS has been used to simulate microgravity in a variety of cell types, including lymphocytes, osteoblasts, and myoblasts[57–59]. The C2C12 cell line used in the experiment presented herein is a mouse myoblast line that can differentiate into contractile skeletal muscle fibers. First cultured in 1977, the C2C12 cell line produces many of the same proteins as human muscle tissue, making it a suitable analog for investigation of radiation and atrophic conditions[60].

Harmful radiation in space primarily comes in two forms, gamma rays and high energy heavy ions[20]. Radiation intensity fluctuates depending on solar activity and proximity to the Earth. The lowest radiation dose rates occur when in close proximity to the Earth and during the solar maximum[20]. Gamma rays are a form of electromagnetic radiation with no mass while high energy heavy ions are atomic nuclei stripped of electrons and moving at relativistic velocities. Some high energy heavy ions are produced by the Sun, but most come from distant supernovae.

Relative biological effectiveness (RBE) is a measure of how damaging a particular type of radiation is to living tissue. Gamma radiation is assigned an RBE of 1 by definition. High energy heavy ions can have RBE values ranging from 20-40,

indicating significantly more tissue damage for an equivalent dose[21]. Although high energy heavy ions present a greater health hazard in spaceflight, they are difficult to simulate in a laboratory and require large particle accelerators to produce. In contrast, gamma radiation sources are relatively inexpensive and a large body of data exists regarding epidemiological studies in radiation-exposed humans, rodents, and non-human primates.

NASA limits astronaut radiation exposure to levels that correspond with a 3% increase in fatal cancer risk[22]. Long term missions beyond low Earth orbit, such as a journey to Mars, exceed this limit within a single mission and increase the risk of developing cancer[20]. Due to the highly penetrating nature of high energy ions in cosmic radiation, shielding the spacecraft is not economically feasible[20]. Biological countermeasures to radiation damage and increased cancer risk provide an attractive alternative to heavy and costly shielding.

One cellular response that counters radiation damage is the up-regulation of heme oxygenase-1 (HO-1)[23, 24]. HO-1 is induced in response to oxidative stress and combats this stress in part by degrading heme into biliverdin-IXα, a natural antioxidant and anti-inflammatory[25]. Artificial induction of HO-1 has demonstrated protective effects against ionizing radiation in multiple tissue types[24, 26]. We hypothesize that the cytoprotective effects of HO-1 are due to downstream biliverdin production from heme catabolism and activation of the phosphatidylinositol 3-kinase (PI3K)-Akt pathway by the biliverdin reductase cell surface receptor. An alternative treatment could include supplementation with vitamin E, which attenuates radiation-induced cell death and scavenges reactive oxygen species[30–32].

Methods

Cell Culture

C2C12 cell stocks were maintained in their undifferentiated state with Dulbecco's Modified Eagles Medium (DMEM) and 10% fetal bovine serum (FBS) from HyClone, GE Healthcare. At passage 7, cells were seeded into the RCCS and control conditions at $2.5x10^5$ cells/mL. Culture conditions were maintained at 37°C and 5% CO_2. Cell counting was performed with a Beckman Coulter ViCell, which uses a Trypan blue exclusion assay. The cells were seeded into DMEM 10% FBS. Every 3 days, the culture media was changed for fresh media. On day 6, the media was changed to DMEM 2% FBS to promote differentiation of the myocytes into myotubes. Experimental cultures were maintained for a total of 15 days. Experimental conditions were normal gravity, normal gravity with radiation, simulated microgravity, and simulated microgravity with radiation. Each condition was cultured in duplicate.

Microgravity Simulation

A Synthecon RCCS-4H with four 10 mL high aspect ratio vessels (HARVs) was used to generate simulated microgravity conditions [Figure 13A]. Cells were cultured on 5 mg/mL of HyClone HyQ Sphere Pplus 102-L microcarrier beads. Rotation of the culture vessels was maintained at 10-12 RPM to prevent settling and maintain cells in a constant state of free-fall. Microcarrier beads in Corning ultra-low attachment tissue culture flasks provide a normal-gravity control. Shear effects from media flow in the RCCS are accounted for by placing the control conditions on an orbital shaker plate at am equivalent RPM [Figure 13B].

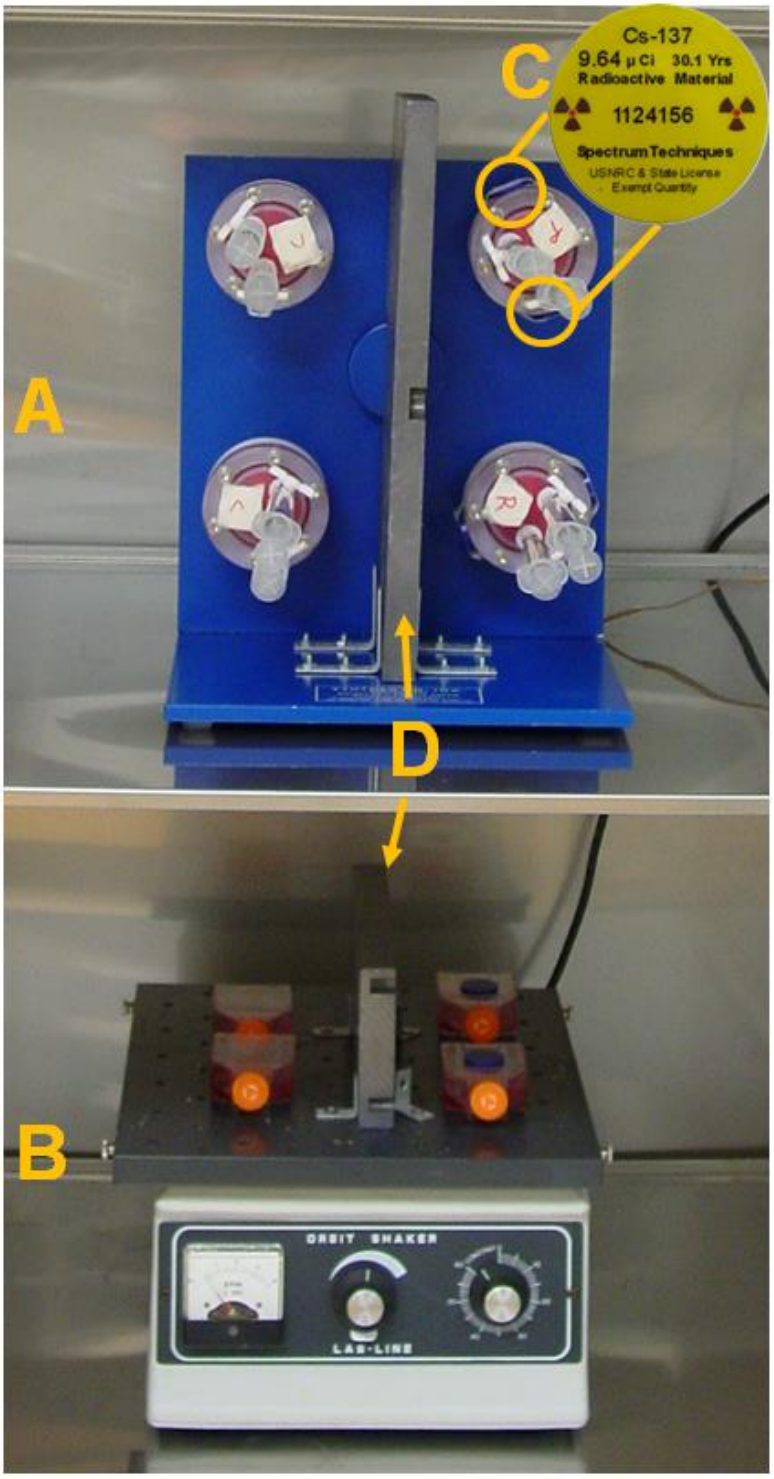

Figure 13. Model setup for microgravity and spaceflight radiation simulation. A – Rotary cell culture system. B – Normal gravity control. C – Cesium-137 source disks. D – Lead shielding.

Radiation Source

Gamma radiation was provided by two Spectrum Technologies cesium-137 source disks attached to the vessels for the duration of the culture [Figure 13C]. The radioactive source disks were approximately 10 µCi, calibrated to ± 5% according to the National Institute of Standards and Technology. Dose rate to the cells was 25-30 µSv/hr. Lead shielding with a thickness of 1.9 cm isolated control conditions from irradiated conditions, reducing dose rate to 0.5-1 µSv/hr [Figure 13D]. Cumulative dose for the 15 day culture was approximately 10 mSv, equivalent to 24 days on the International Space station[76].

Spent Media Analysis

Amino acid concentrations in cell culture media from day 15 were determined with a Waters Alliance 2695 high performance liquid chromatography (HPLC) system. Analysis of alanine and the branch chain amino acids (BCAAs) leucine, isoleucine, and valine was conducted. Alanine is secreted into the bloodstream by muscle fibers while BCAAs are oxidized for nutrients[74, 75]. Lower alanine and BCAA consumption would indicate decreased metabolic activity, expected in simulated microgravity and irradiated conditions.

Fluorescent Imaging

Cell morphology, viability, lipid peroxidation, and DNA damage were determined via fluorescent imaging with a Zeiss confocal microscope. We expect decreased viability, increased lipid peroxidation from ROS, and double-strand DNA breaks in irradiated conditions. Simulated microgravity it expected to increase lipid peroxidation due to ROS. For live cell assays, the cells were rinsed with phosphate buffered saline (PBS) and

incubated with the dyes for 30 minutes at 37°C before imaging. Live cell imaging for viability used 1 µM Hoechst 33342, 2.5 µM propidium iodide, and 3 µM Calcein-AM. Live cell imaging for lipid peroxidation used 1 µM Hoechst 33342, 50 nM MitoTracker CMX-Ros, and 20 µM dichloro-dihydrofluorescein (DCF).

For the fixed cell DNA damage H2AX assay, cells were first incubated in DMEM with 50 nM Mitotracker CMX-Ros for 30 minutes at 37°C. The media was removed and PBS containing 4% paraformaldehyde was added for 15 minutes at room temperature to fix the cells. The cells were rinsed once with PBS and then permeabilized with 2.5 µL/mL of Triton X-100 in PBS for 15 minutes at room temperature. The fixation buffer was removed, the cells rinsed again in PBS, and then blocked for one hour with 10 mg/mL of bovine serum albumin in PBS at room temperature to prevent non-specific binding of the primary antibody. After removing the blocking buffer, the 2 µg/mL of Anti-phospho-Histone H2AX (Ser139) primary antibody from Millipore, diluted in blocking buffer, was added for one hour at room temperature. The cells were then rinsed three times with PBS before adding 1 µg/mL of goat anti-mouse IgG (H+L) secondary antibody conjugated with Alexa Fluor 488, from Thermo Fisher Scientific. The secondary antibody was diluted in blocking buffer, along with Hoechst 33342, and incubated for one hour at room temperature. Finally, the cells were rinsed again three times with PBS and imaged.

Western Blot

Protein analysis was accomplished using Western blot. Lower concentrations of the muscle proteins myosin and tropomyosin are expected in simulated microgravity and irradiated conditions. Intracellular proteins were extracted by lysing the cells while

adhered to the microcarrier beads. Cells were rinsed with PBS and lysed using a urea based lysis buffer containing 8M urea, 300mM NaCl, 5mL/L Triton X-100, 50mM sodium phosphate dibasic, and 50mM Tris-HCl. A protease inhibitor cocktail consisting of 1mM PMSF and 0.1mg/mL of pepstatin, antipain, and leupeptin was added to the lysis buffer.

Lysate protein content was determined using a Pierce BCA protein assay kit and a Thermo Scientific NanoDrop. SDS PAGE was performed using pre-cast 4-20% Tris-Glycine gels from NuSep. 20 µg of each sample was loaded onto the gel along with 10 µg of actin and myosin standard from BioRad. After running at 150 V for one hour, the proteins were transferred to a PVDF membrane using a Pierce fast semi-dry blotter according to the manufacturer instructions. Primary antibodies MF-20 and CH-1, which have activity against myosin and tropomyosin, respectively, were purchased from the Developmental Studies Hybridoma Bank. Antibody concentration was 0.35 µg/mL. Antibody incubation was performed according to published protocol[77]. The blot was developed with SuperSignal West Pico Chemiluminescent substrate from Thermo Scientific and imaged with a Thermo Scientific myECL imager.

Enzyme Linked Immunosorbent Assay

HO-1 was assayed with an IMMUNOSET HO-1 (mouse) ELISA development set from Enzo Life Sciences. From the cell lysate, 20 µg of total protein, as determined by BCA assay, was loaded into each well. The plate was developed with 1-Step Turbo TMB-ELISA substrate from Thermo Scientific and imaged with a SpectraMax M2 plate reader.

Results and Discussion

Spent Media Analysis

Slight decreases in alanine concentration for radiation exposed conditions were observed [Figure 14]. Alanine is not present in DMEM and is released by muscle fibers into the media as part of the alanine cycle[74]. Reduced alanine secretion indicates fewer muscle fibers and/or lower metabolic activity, expected for cells under increased stress or atrophic conditions. Reduced alanine in radiation exposed conditions was in line with expectations. On the other hand, alanine concentrations in simulated microgravity vs. normal gravity controls did not follow the expected trend. Cells cultured in simulated microgravity had higher extracellular alanine concentrations than the normal gravity controls. Increased sample size is necessary to determine if these results are statistically significant.

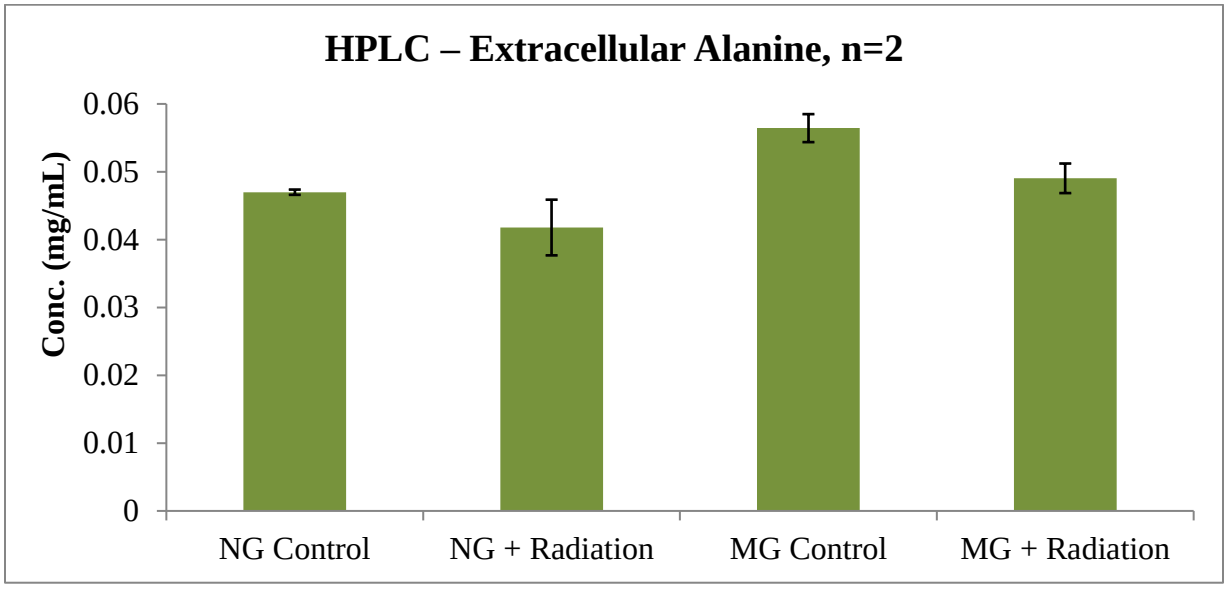

Figure 14. Alanine concentrations in spent media harvested on day 15. NG = normal gravity. MG = microgravity. Error bars are high/low for n=2.

No significant differences were observed in the concentration of BCAAs. BCAAs are oxidized during muscle fiber activity[75]. We expected to observe decreased BCAA consumption in conditions exposed to simulated microgravity. Similar BCAA consumption across all conditions may be due to insufficient sample size and/or culture time.

Fluorescent Imaging

Fluorescent imaging for cell viability did not reveal significant differences between conditions. Differentiation of myocytes into multi-nucleated myotubes was confirmed for all conditions, demonstrating that simulated microgravity does not prohibit formation of new muscle fibers. Lipid peroxidation was observed in both normal gravity controls and simulated microgravity conditions, as indicated by DCF [Figures 15-16]. Radiation provided by the cesium-137 sources induced minor double-strand DNA breaks, as visualized by H2AX phosphorylation[78] [Figures 17-18]. Stronger radiation sources are being investigated to provide more significant damage.

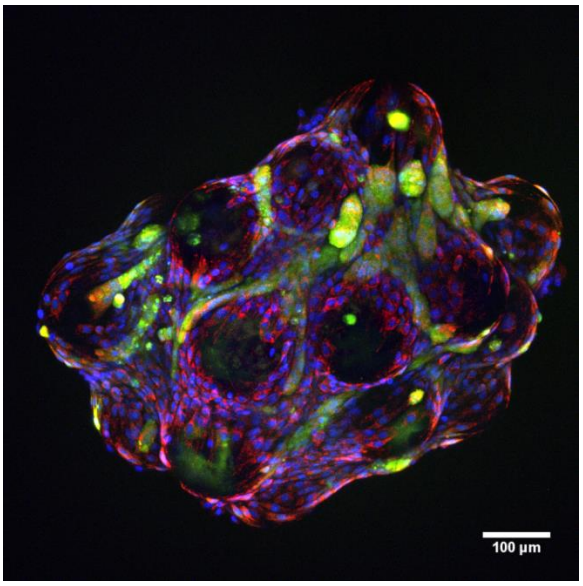

Figure 15. Normal gravity control stained for nuclei with Hoechst (blue), muscle fibers with MitoTracker (red), and lipid peroxidation with DCF (green).

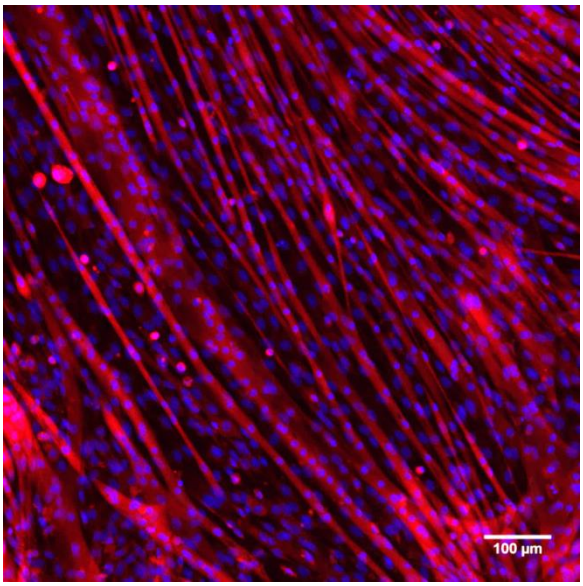

Figure 17. No-radiation control under normal gravity stained for nuclei with Hoechst (blue), muscle fibers with MitoTracker (red), and H2AX phosphorylation (green, not present).

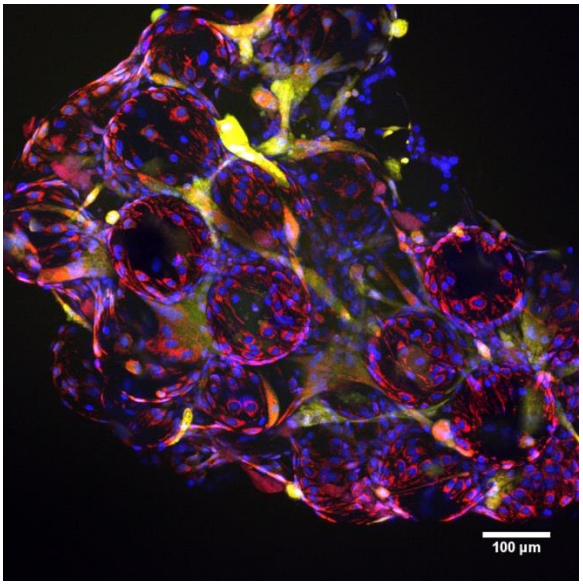

Figure 16. Simulated microgravity control stained for nuclei with Hoechst (blue), muscle fibers with MitoTracker (red), and lipid peroxidation with DCF (green).

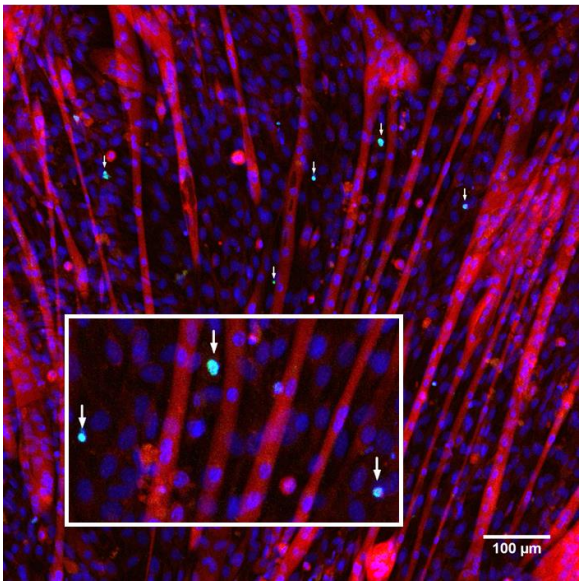

Figure 18. Radiation exposed condition under normal gravity stained for nuclei with Hoechst (blue), muscle fibers with MitoTracker (red), and H2AX phosphorylation (green, see inset for detail).

Enzyme Linked Immunosorbent Assay for Heme Oxygenase-1

HO-1 is upregulated during periods of oxidative stress to catabolize heme into biliverdin, a natural antioxidant[79]. Due to oxidative stress induced by radiation and the microgravity environment, we expected to observe an increase in HO-1 for radiation-exposed conditions as well as cell cultured in simulated microgravity. However, decreased HO-1 in cell lysate was observed for radiation-exposed conditions [Figure 19]. The large error bars preclude drawing conclusions regarding HO-1 in simulated microgravity vs. normal-gravity controls until more data is generated. To maximize protein concentration, undiluted lysate was used for the assay. Error may be introduced due to the high viscosity of the lysate, resulting in inconsistent pipetting.

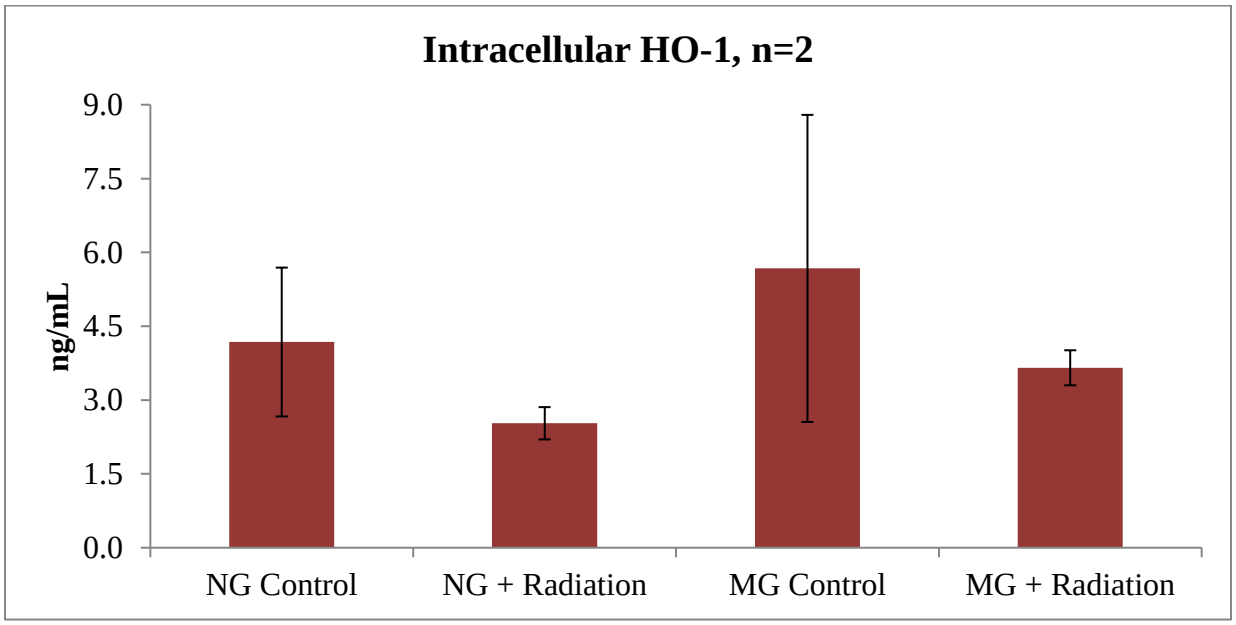

Figure 19. HO-1 ELISA with cell lysate containing 20 µg total protein. NG = normal gravity. MG = microgravity. Error bars are high/low for n=2.

Proposed Atrophy and Radiation Countermeasures

Successful development of a ground-based model for microgravity-induced muscle atrophy and spaceflight radiation would provide a low-cost platform for testing anti-atrophy and radioprotective drugs. We have identified promising therapeutic compounds to counter cellular damage from spaceflight conditions. A major contributor to muscular atrophy is the increased production of tissue-damaging reactive oxygen species following immobilization or disuse, including disuse stemming from the microgravity conditions of spaceflight[80–82]. Hydrogen peroxide (H_2O_2) released from murine mitochondria nearly doubles after two weeks of hind limb suspension, which in addition to its inherent cytotoxic effects stimulates the release of calpain and Caspase 3, proteases that degrade myofilaments[83]. Exposure to ionizing radiation also generates reactive oxygen species via radiolysis of water[19]. Scavenging these reactive oxygen species would limit calpain and Caspase 3 activation and protect cells from damage.

Mesobiliverdin-IXα

To combat the oxidative stress associated with disuse atrophy of skeletal muscle, we propose mesobiliverdin-IXα, a microbial-sourced analog of biliverdin-IXα with antioxidant and anti-inflammatory properties. Biliverdin-IXα cannot be economically extracted from mammalian cells due to rapid conversion to bilirubin by biliverdin reductase. However, we have isolated gram quantities of mesobiliverdin-IXα from cyanobacteria bile pigments using a scalable process. Mesobiliverdin-IXα was found to behave similarly to biliverdin-IXα, including serving as a substrate biliverdin reductase in human cells[84]. Cytoprotective effects of mesobiliverdin-IXα and biliverdin analogs have been demonstrated with pancreatic islet cells, vascular endothelial cells, and arterial smooth muscle cells[84–86].

Our preliminary data indicates increased protein production in both normal gravity and simulated microgravity conditions for cells supplemented with 10 μM of mesobiliverdin-IXα, as determined by Western blot [Figure 20]. The normal gravity control in this example performed worse than expected, likely due to mechanical stress from a rocker plate. Current controls are cultured on an orbital shaker with a fluid motion more similar to that of the RCCS.

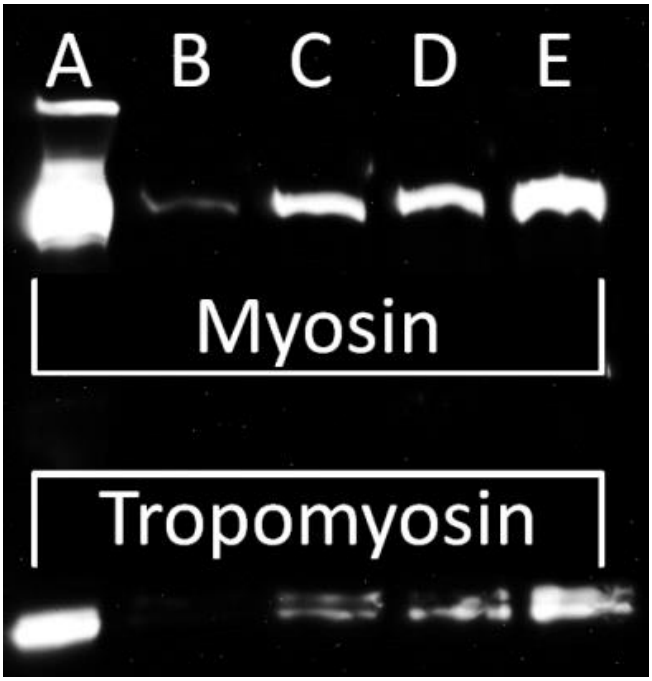

Figure 20. A – Myosin and tropomyosin standard. B – Normal gravity control. C – Normal gravity control with 10 μM mesobiliverdin-IXα. D – Microgravity control. E – Microgravity with 10 μM mesobiliverdin-IXα.

The direct antioxidant properties of bilirubin and biliverdin-IXα in cell-free systems have been established[87]. We hypothesize that mesobiliverdin-IXα will exhibit indirect cytoprotection by moderating expression of heme oxygenase-1, an inducible enzyme which combats oxidative stress in part by degrading heme into biliverdin-IXα[25]. Elucidating the

influence of mesobiliverdin-IXα on HO-1 is critical due to the numerous downstream effects of HO-1 activation. Increasing HO-1 expression with hemin supplementation attenuates immobilization-induced skeletal muscle atrophy, potentially by preventing protein degradation from oxidative stress[88].

However, not all of the products of heme degradation are beneficial. In addition to biliverdin-IXα, heme degradation also results in the production of carbon monoxide (CO) and iron (Fe^{2+}) [Figure 21]. Contrary to the antioxidant properties of biliverdin-IXα, free Fe^{2+} can react with H_2O_2 to produce a hydroxyl radical[18]. Furthermore, CO inhibits CCAAT-enhancer-binding protein δ from binding to the MyoD promoter [Figure 21], thereby reducing the differentiation of myoblasts into contractile myotubes[89]. This side effect of the HO-1 oxidative stress response mechanism is especially detrimental in spaceflight, where significant muscle loss is experienced despite the current International Space Station exercise program[90].

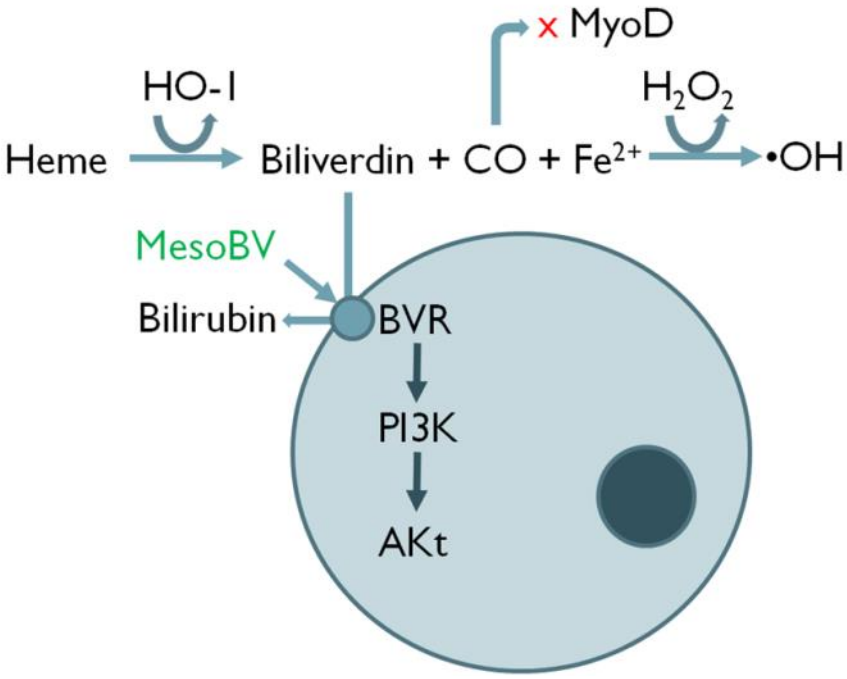

Figure 21. Heme catabolism pathway with proposed mesobiliverdin route of efficacy

Mesobiliverdin-IXα may provide the cytoprotective effects of HO-1 without induction of MyoD inhibition and Fe^{2+} generation. Activation of cell-surface biliverdin reductase (BVR) has important downstream consequences, inducing Akt via intracellular phosphorylation of BVR, which binds to the p85α subunit of PI3K[91]. PI3K activation suppresses phosphatase and tensin homolog (PTEN), a negative regulator of muscle growth[92]. Furthermore, Akt regulated protein synthesis pathways are inhibited during periods of inactivity[92]. Activation of the PI3K-Akt pathway also limits cellular apoptosis following irradiation[93, 94]. Since mesobiliverdin-IXα serves as a substrate for human BVR[84], we hypothesize that supplementation with mesobiliverdin-IXα will provide the benefits of increased PI3K and Akt expression. The prospective action of mesobiliverdin-IXα through the BVR—PI3K—Akt pathway is encouraging. Activating Akt directly causes feedback inhibition of PI3K, associated with cardiac dilation and death in the long-term[95, 96]. Since mesobiliverdin-IXα's action on Akt would be indirect, we do not anticipate the aforementioned complications.

It will be critical to determine if mesobiliverdin-IXα inhibits HO-1 via a feedback mechanism. The breakdown of heme is important, as excess heme produces inflammation and apoptosis in a variety of cell types[97, 98]. If, upon mesobiliverdin-IXα supplementation, HO-1 induction is lessened in response to oxidative stress but not in response to free heme, MyoD-inhibiting CO and generation of hydroxyl radicals from Fe^{2+} will be limited while both the direct antioxidant properties of mesobiliverdin-IXα and downstream BVR—PI3K—Akt pathways are maintained.

Vitamin E

Another promising atrophy and radiation countermeasure is vitamin E. The antioxidant effects of vitamin E scavenge free radicals and reduce expression of calpains and Caspase 3, -9,

and -12, reducing muscular atrophy due to immobilization and unloading[27, 28]. In addition to preventing muscle loss, vitamin E also preserves bone mass and strength following unloading[29]. Several forms of vitamin E have demonstrated radioprotective effects, including α-tocopherol, δ-tocotrienol, and γ-tocotrienol[30–32]. Unlike mesobiliverdin-IXα, vitamin E inhibits the PI3K-Akt pathway, which may promote apoptosis of tumor cells[99, 100]. The effects of combined mesobiliverdin-IXα and vitamin E supplementation will also be investigated.

Conclusions

The RCCS successfully cultures and permits differentiation of multi-nucleated myotubes, basic components of muscle tissue. Irradiation for 15 days with 20 μCi of cesium-137 produces minimal double-stranded DNA breaks. Exposure to radiation resulted in decreased concentrations of alanine and HO-1, though more data must be generated to determine statistical significance. Stronger radiation sources are being investigated to provide a dose equivalent to a journey to Mars within a two week culture period.

The initial data generated since January 2015 are insufficient to determine whether or not the combination of a RCCS and radiation source provide a platform that generates conditions mimicking spaceflight. To conclusively demonstrate similarity of the model to spaceflight, muscle protein concentration must be lower and markers of oxidative stress must be higher in microgravity and irradiated conditions. Increased expression of the atrophy markers Atrogen-1, MuRF1, and Nedd4 in simulated microgravity would provide evidence of the model's effectiveness[101]. Analysis of these markers with qRT-PCR is ongoing. Culture on flat membranes instead of microcarrier beads may improve fluorescent imaging results. The Z-stacks

required for 3D bead clusters can take more than one hour per image, leaving ample time for cells to undergo changes when performing live cell imaging.

Completion of an *in vitro* ground-based model for spaceflight atrophy and radiation injury would provide a valuable platform for testing countermeasures necessary to ensure astronaut health and fitness during long-term spaceflight. Radiation doses can be tuned to simulate a variety of mission circumstances from short-term low Earth orbit to multi-year expeditions on Mars. The metrics presented herein will also elucidate the mechanisms of action for atrophy and radiation countermeasures, providing a foundation for design and selection of novel therapeutics.

CHAPTER 5

FINAL MANUSCRIPT

Muscle atrophy marker expression differs between rotary cell culture system and animal studies

Abstract

Muscular atrophy, defined as the loss of muscle tissue, is a serious issue for immobilized patients on Earth and in human spaceflight, where microgravity prevents normal muscle loading. *In vitro* modeling is an important step in understanding atrophy mechanisms and testing countermeasures before animal trials. The most ideal environment for modeling must be empirically determined to best mimic known responses *in vivo*.

To simulate microgravity conditions, murine C2C12 myoblasts were cultured in a rotary cell culture system (RCCS). Alginate encapsulation was compared against polystyrene microcarrier beads as a substrate for culturing these adherent muscle cells. Changes after culture under simulated microgravity were characterized by assessing mRNA expression of MuRF1, MAFbx, Caspase 3, Akt2, mTOR, Ankrd1, and Foxo3. Protein concentration of myosin heavy chain 4 (Myh4) was used as a differentiation marker. Cell morphology and substrate structure were evaluated with brightfield and fluorescent imaging.

Differentiated C2C12 cells encapsulated in alginate had a significant increase in only MuRF1 following simulated microgravity culture and were morphologically dissimilar to normal cultured muscle tissue. On the other hand, C2C12 cells cultured on polystyrene microcarriers had significantly increased expression of MuRF1, Caspase 3, and Foxo3 and easily identifiable multi-nucleated myotubes. The extent of differentiation was higher in simulated microgravity and protein synthesis more active with increased Myh4, Akt2, and mTOR. The *in vitro*

microcarrier model described herein significantly increases expression of several of the same atrophy markers as *in vivo* models. However, unlike animal models, MAFbx and Ankrd1 were not significantly increased and the fold change in MuRF1 and Foxo3 was lower than expected. Using a standard commercially available RCCS, the substrates and culture methods described only partially model changes in mRNAs associated with atrophy *in vivo*.

Introduction

Muscle loss from disuse negatively affects quality of life in patients on Earth and remains a significant risk factor to astronaut health despite rigorous exercise programs onboard the International Space Station[102, 8]. Approximately 40-50% of total body mass is skeletal muscle and its loss can induce numerous detrimental physiological changes, including reduced power, lower endurance, and atypical reflex responses[6, 7]. Disuse, reduced protein synthesis, and reduced motor neuron activity all contribute to losing muscle tissue and strength in spaceflight[6]. Atrophy severity varies with microgravity exposure time and anatomical region. Muscle mass loss for short duration missions ranges from 10-20%, compared to 30-50% for long duration missions[2, 3]. To reduce these risks, flight protocol at the National Aeronautics and Space Administration (NASA) mandates that crew members exercise on missions lasting over 10 days; however, loss of strength and muscle mass has been reported after only 5 days[4, 5]. Preserving astronaut strength and endurance by limiting muscle atrophy is critical for enabling long duration space travel and exploration. To this end, ground-based modeling of microgravity is a critical step in developing atrophy countermeasures.

Three key mRNAs in muscle loss are muscle RING finger-1 (MuRF1, also called Trim63), muscle atrophy F-box (MAFbx, also called Fbxo32 and Atrogin-1), and Caspase 3, all upregulated in numerous rodent models of muscular atrophy including disease, immobilization,

hind limb unloading, as well as spaceflight[12, 15, 34–45]. MuRF1 and MAFbx are key E3 ubiquitin ligases involved in recycling of muscle proteins[12]. However, intact muscle fibers cannot be degraded by the ubiquitin proteasome system and must be broken down before MuRF1 and MAFbx can act. This breakdown is induced by Caspase 3, upregulated during muscular atrophy and responsible for the degradation of actomyosin complexes in the muscle tissue[7, 11]. Following hind limb unloading, knockout mice lacking MuRF1 and MAFbx display significantly less atrophy than wild type mice, highlighting the importance of those ligases in the mechanisms underlying muscle loss[12, 35].

Additional mRNAs important for monitoring muscle health include Akt2, Foxo3, mTOR, and Ankrd1. Akt2 (also called Protein Kinase B β) is a serine/threonine-protein kinase and a downstream target of insulin-like growth factor (IGF) induced muscle differentiation[103]. Upregulated significantly in differentiated skeletal muscle, the absence of Akt2 leads to a substantial reduction in myotube diameter[104]. Forkhead Box O3 (Foxo3), another downstream target of the IGF signaling pathway, is also upregulated during muscle atrophy *in vitro* and *in vivo*[105–107]. Foxo3 is responsible for activation of multiple atrophy-related transcription factors, including the ubiquitin ligase MAFbx[107]. A third component of the IGF signaling pathway is mammalian target of rapamycin (mTOR), a regulator of protein synthesis and muscle hypertrophy that is increased by mechanical stimulation and in the presence of nutrients and growth factors[108, 109]. Unlike the previously discussed mRNAs, mTOR expression decreases during muscle atrophy as the ubiquitin proteasome system becomes more active.

Finally, cardiac ankyrin repeat protein (Ankrd1, also called CARP) is upregulated in both unloading and denervation models *in vivo*[106, 110]. The increase in Ankrd1 expression during muscular atrophy has been reported as up to an order of magnitude higher than that of other

markers such as MAFbx and MuRF1[110]. Furthermore, the aforementioned proteasome-related markers may only be temporarily upregulated during the initial stages of muscle atrophy, where Ankrd1 is persistently expressed at high levels[110]. The large, easily detected increase in Ankrd1 makes it an attractive target for evaluating muscular atrophy models.

A classic method for simulating weightlessness is the hind limb unloading rodent model, developed at NASA in the 1970's[33]. In this model, the rodent is affixed in a harness or tail traction device such that the hind limbs are elevated at a 30° angle[33]. The resulting unloading induces muscle atrophy in the hind limbs and cephalic fluid shift similar to real microgravity conditions[33]. However, ground-based animal models differ from human physiology, are more time consuming, more expensive, and are subject to more regulation than cell culture models, providing strong motivation to develop other methods. Newly developed therapeutics can be effectively screened with smaller quantities in cell culture models and safe dose ranges established prior to testing *in vivo*. Highly tissue-specific effects can be elucidated without confounding variables introduced by other systems in the organism. Additionally, cell culture models enable use of primary human cell lines, increasing biological relevance to humans.

In vitro modeling of microgravity can be conducted with rotary culture systems and three-dimensional random positioning machines or clinostats[54, 55]. Here, we employ the RCCS, developed by Synthecon Inc. in conjunction with NASA to simulate microgravity[54]. In the RCCS, microgravity is mimicked by the rotational motion of the vessel maintaining cells at their terminal settling velocity, similar to what astronauts experience in orbit around Earth. The RCCS has been used to simulate microgravity in a variety of cell types, such as lymphocytes, osteoblasts, and myoblasts, including the C2C12 mouse myoblast cell line used herein[56–59, 73, 111]. The C2C12 cell line differentiates into contractile skeletal muscle fibers and produces

many of the same proteins and mRNAs as human muscle tissue[60]. Use of a mouse cell line for *in vitro* model development and extension also benefits from a large body of literature available on mRNA expression in live mouse microgravity models, providing information for evaluating the model's similarity to *in vivo* studies. Previously published work with muscle cells, including C2C12s, in simulated microgravity focused on changes in differentiation induced by culture in the RCCS[56, 59, 73]. To the best of the authors' knowledge, no previously published work has investigated changes in atrophy-specific mRNAs with muscle cell culture in the RCCS.

Standard culture methods for adherent cells in the RCCS employ a substrate to support growth. Two substrates commonly used in three-dimensional cell culture are microcarrier beads and alginate encapsulation. Microcarriers are an attractive substrate due to ease of scalability for producing large quantities of cells for therapeutic applications[69, 70]. As in standard tissue culture flasks, C2C12 cells differentiate on microcarriers *in vitro.* The beads offer a wide variety of surface chemistries tailored to specific cell types and culture conditions[69].

Alternatively, adherent cells can be encapsulated within a several synthetic or naturally occurring hydrogels[61]. Naturally occurring alginate hydrogel has well established uses for mammalian cell encapsulation due to low toxicity and gentle gelling conditions[61–66]. Additionally, the high porosity of alginate hydrogels is advantageous for maximizing diffusion rates and ensuring adequate exchange of nutrients and waste products with the surrounding culture media[62]. In contrast with microcarrier beads, which can only be seeded with undifferentiated cells, alginate encapsulation can be performed on both undifferentiated and differentiated muscle cells. The percentage alginate used for encapsulation can be varied between 1.5-3% (w/v) depending on the cell type and desired mechanical properties[63–66, 68].

To preserve bead integrity in the dynamic RCCS environment, we elected to encapsulate cells at the upper end of this range to maximize mechanical strength of the beads[62].

Here, we propose a ground-based protocol using C2C12 cells and a RCCS to induce expression of the atrophy-related mRNAs MuRF1, Caspase 3, and Foxo3. Additionally, the model induces significant changes in Akt2 and mTOR expression. The model is limited by a lack of significant MAFbx and Ankrd1 expression and low fold changes in MuRF1 and Foxo3. While not currently suitable for these purposes, with further development we expect that the RCCS can be improved to more closely match the expression changes of animal hind limb unloading models.

Materials and Methods

Cell Culture

C2C12 (ATCC CRL-1772, Manassas, VA, USA) cell stocks were maintained in their undifferentiated state with Dulbecco's Modified Eagles Medium (DMEM) and 10% fetal bovine serum (FBS) from HyClone, GE Healthcare (Logan, UT, USA). Stocks were passaged at 60-70% confluency during scale-up. Cell counting prior to seeding was performed with a Beckman Coulter Vi-Cell (Indianapolis, IN, USA), which uses a trypan blue exclusion assay. The experimental conditions consisted of four replicated vessels per run for each condition described in Table 1. Controls consisted of standard T25 tissue culture flasks for alginate encapsulated conditions and ultra-low attachment (ULA) tissue culture flasks (Corning, NY, USA) for microcarrier conditions.

Table 1. Experimental conditions. All cultures had a total duration of 15 days.

Substrate	Cell State at Seeding	Culture Vessel
Alginate	Undifferentiated	Standard T25 (Control)
Alginate	Undifferentiated	RCCS
Alginate	Differentiated	Standard T25 (Control)

Alginate	Differentiated	RCCS
Microcarrier	Undifferentiated	ULA T25 (Control)
Microcarrier	Undifferentiated	RCCS
Microcarrier	Undifferentiated	Horizontally orientated RCCS (Control)
Microcarrier	Undifferentiated	ULA T25 Days 1-12, RCCS Days 13-15

The use of ultra-low attachment flasks for microcarrier cultures was necessary to prevent cells from growing on the flask surface, forcing adherence on the microcarrier beads and ensuring the available surface area for cell growth was identical to the RCCS vessels. Cells were seeded into each experimental condition of Table 1 at $2.5x10^5$ cells mL^{-1} with a total volume of 10 mL. Culture conditions were maintained at 37°C and 5% CO_2. Every 3 days, the culture media was changed for fresh media. On day 6, the media was changed to DMEM 2% FBS to promote differentiation of the myocytes into myotubes. All cultures were maintained for a total of 15 days. The 15 day culture time was selected to maximize exposure to the simulated microgravity environment while preventing loss of cell attachment from microcarriers, previously reported for longer duration cultures[112]. For the final condition in Table 1, the cells were moved from ULA T25s to the RCCS for the final 3 days of the culture period.

Microgravity Simulation

A Synthecon RCCS-4H (Houston, TX, USA) with four 10 mL high-aspect-ratio vessels (HARVs) was used to generate simulated microgravity conditions. Sterilization and operation of the Synthecon RCCS-4H was carried out in accordance with the manufacturer's instructions. Vessel rotation was adjusted empirically to maintain the majority of the substrate in suspension, as described in Table 2. The horizontally orientated RCCS, investigated as a normal gravity control, was maintained at the mean RPM of 15. When the substrates are maintained at their terminal settling velocity, the force of gravity F_g is described by Stoke's Law (Equation 1).

$$F_g = (\rho_a - \rho) g \frac{4}{3} \pi R^3 \quad (1)$$

In Equation 1, ρ_a is the density of the cell aggregate, ρ is the density of the culture media, R is the radius of the cell aggregate and g is the force of gravity. The resulting F_g is balanced by the drag force from the rotating fluid, resulting in a net force of zero. Since g and R are constant at any given moment, the ratio of F_g in the RCCS to the normal force of gravity can be simplified to express how many times normal gravity (Xg) is produced within the system, as described by Equation 2 and detailed in Table 2.

$$Xg = \frac{F_{g\,RCCS}}{F_{g\,Normal}} = \frac{\rho_a - \rho}{\rho_a} \quad (2)$$

Table 2. The RCCS rotation rate necessary to maintain the substrates in suspension varies with diameter. Times Earth Gravity varies with substrate density. [a]Microcarrier initial diameter at seeding. [b]Microcarrier cluster diameter at harvest. Data displayed as mean ± CV, n=10.

Substrate	Density (g cm^{-3})	Xg	Diameter (µm)	RPM
Microcarriers	1.02	0.02	160±18.7%[a] to 698±10.5%[b]	10-20
Alginate	1.07	0.07	3252±3.2%	35

Microcarriers

Undifferentiated C2C12 cells were cultured on 5 mg mL^{-1} of HyClone HyQ Sphere Pplus 102-L microcarrier beads. These polystyrene beads have a cationic surface charge and are well suited for culturing cells in agitated vessels with serum-containing media[69]. Rotation of the culture vessels was initiated at 10 RPM and increased up to 20 RPM as the culture age increased and amalgamations of beads formed. Vessel RPM was adjusted empirically to prevent settling and maintain the beads suspended at their terminal settling velocity. Microcarrier beads in static

ULA T25 tissue culture flasks provided a normal-gravity control and produced microcarrier cluster sizes similar to those in the RCCS.

Alginate Encapsulation

Undifferentiated C2C12 cells were mixed with 3% (w/v) solution of high viscosity alginate (MP Biomedicals, Santa Ana, CA, USA) at a density of $10x10^6$ cells mL^{-1}. Beads were formed by dripping the alginate-cell mixture into 200 mM $CaCl_2$ 10mM HEPES at pH 7 through a 19-gauge syringe needle at a flow rate of 2 mL min^{-1}. The beads were cured in $CaCl_2$ buffer for 20 minutes at 37°C. Once cured, the average bead diameter was 3252±103 µm with a volume of approximately 18 µL, yielding $1.8x10^5$ cells per bead. To match the seed volume of the microcarriers, 14 alginate beads were used per 10 mL vessel. The beads were rinsed once with DPBS and transferred to their respective culture conditions in DMEM 10% FBS.

Differentiated cells were encapsulated following 9 days of growth in standard tissue culture flasks. The myotubes were removed from the flask with a cell scraper and re-suspended at a density of 75 cm^2 culture area per mL of alginate. Subsequent alginate encapsulation methods were performed as described for undifferentiated cells.

Upon harvest, the alginate beads were dissolved with 100 mM sodium citrate, 150 mM NaCl, 30 mM EDTA at pH 7.0 and 37°C. The cells were pelleted via centrifugation and rinsed with DPBS before proceeding with RNA extraction, as described in the following section.

Atrophy Marker Expression

Relative expression of the atrophy markers MuRF1, MAFbx, and Caspase 3 was determined using RT^2 qPCR primer assays from Qiagen (Hilden, Germany). Akt2, mTOR, Foxo3, and Ankrd1 primers were purchased from Bio Rad (Hercules, CA, USA). RNA extraction was carried out immediately upon culture harvest using the illustra RNAspin Mini Kit

according to the manufacturer's instructions (GE Healthcare, Marlborough, MA, USA). Extracted RNA was quantified with a NanoDrop (Thermo Fisher Scientific, Waltham, MA, USA) and converted to cDNA with the RT^2 First Strand Kit from Qiagen. All PCR reactions were loaded with 5 ng of cDNA and SYBR Green ROX qPCR Mastermix from Qiagen. Fluorescence was read with an Eppendorf Mastercycler realplex4 (Hamburg, Germany). Cycle settings were 95°C for 10 minutes, followed by 40 cycles of 95°C for 15 seconds, then 60°C for 1 minute. Analysis was performed using the default noise band threshold with drift correction applied in Eppendorf Mastercycler realplex 2.2 software. All results were normalized to glyceraldehyde 3-phosphate dehydrogenase (GAPDH), a suitable housekeeping gene for atrophying muscle tissue *in vitro* and *in vivo*[113–118]. GAPDH expression in our samples was stable, with a CV of 2.5% for all microcarrier samples and 3.7% for all alginate samples. Normalization was calculated with the $2^{\Delta\Delta Ct}$ method[119].

Microscopy

Brightfield microscopy was performed using an AMG EVOS xl from Thermo Fisher Scientific to assess encapsulated cell distribution and alginate bead size and shape. The beads were then fixed in cold methanol for 30 minutes at -20°C, transferred to a solution of 30% sucrose 0.1M $CaCl_2$ overnight at 4°C, then frozen in Tissue-Plus O.C.T. compound (Fisher Scientific, Pittsburg, PA, USA) at -20°C until sectioning[120]. Using a Leica CM1850 cryo-microtome (Wetzlar, Germany), the beads were sliced into 30 µm sections and mounted on Fisher SuperFrost Plus slides, treated with 1 µM Hoechst 33342 (Invitrogen, Carlsbad, CA, USA) to visualize the nuclei and imaged with an Observer Z1 confocal microscope (Zeiss, Oberkochen, Germany).

Cell morphology for microcarriers was also evaluated via fluorescent imaging with the Observer Z1 confocal microscope. Microcarrier-cell clusters were first rinsed with DPBS, then incubated with 1 µM Hoechst 33342 and 50 nM MitoTracker CMX-Ros (Invitrogen, Carlsbad, CA, USA) for 1 hour at 37°C. The clusters were rinsed again with DPBS and z-stack images were acquired with a 3 µm step size. Diameter of multi-nucleated muscle fibers growing on the microcarriers was determined with ImageJ.

Protein Assay

Extent of terminal differentiation was quantified by ELISA for mouse myosin heavy chain 4 (Myh4) (Biomatik, Wilmington, DE, USA), present in high levels in fused myotubes[121]. Cells were rinsed with PBS and lysed using a urea-based lysis buffer containing 8 M urea, 300 mM NaCl, 5mL L^{-1} Triton X-100, 50 mM sodium phosphate dibasic, and 50 mM Tris-HCl. A protease inhibitor cocktail consisting of 1 mM PMSF and 0.1mg mL^{-1} of pepstatin, antipain, and leupeptin was added to the lysis buffer. The cells were lysed on the microcarriers and the lysate was isolated by centrifugation. Lysate protein content was determined using a BCA protein assay kit (Pierce, Rockford, IL, USA) and a SpectraMax i3x (Molecular Devices, San Jose, CA, USA). Lysates were diluted to 1 µg mL^{-1} total protein with PBS and the ELISA kit ran according to the manufacturer's instructions. Quantitation was performed using the Spectramax i3x.

Statistics

Graphical data are presented as the means ± standard deviation. Significance was determined by comparing data sets with Student's t-test. Differences were considered significant at $P < 0.05$.

Results

Microcarrier Substrate Structure & Cell Morphology

When cultured on HyQSphere Pplus 102-L microcarriers, C2C12 cells form monolayers over the bead surface (Figure 22). Differentiated, multi-nucleated myotubes were observed spanning across beads (Figure 22A, C). No significant difference was observed in differentiation or number of multi-nucleated myotubes between simulated microgravity and normal gravity controls. The irregular three-dimensional structure of the bead amalgamations was best visualized with brightfield microscopy (Figure 22B, D). Microcarrier bead cluster size increased with culture age in both normal gravity controls and simulated microgravity conditions. Due to the lack of agitation, maximum cluster size was larger in normal gravity controls than in the RCCS. Additionally, bead clusters formed in normal gravity had widely varying, irregular shapes compared to consistently rounded bead clusters formed in the RCCS (Figure 22 A, B vs. C, D). Despite variations in cluster size and shape, no significant differences in cell morphology were observed. Muscle fiber diameter was 12.7±6.0 μm and 9.5±1.7 μm for normal gravity controls and simulated microgravity conditions, respectively. Fiber diameters were more consistent in the RCCS, but the difference between conditions was not significant ($p>0.05$, $n=10$).

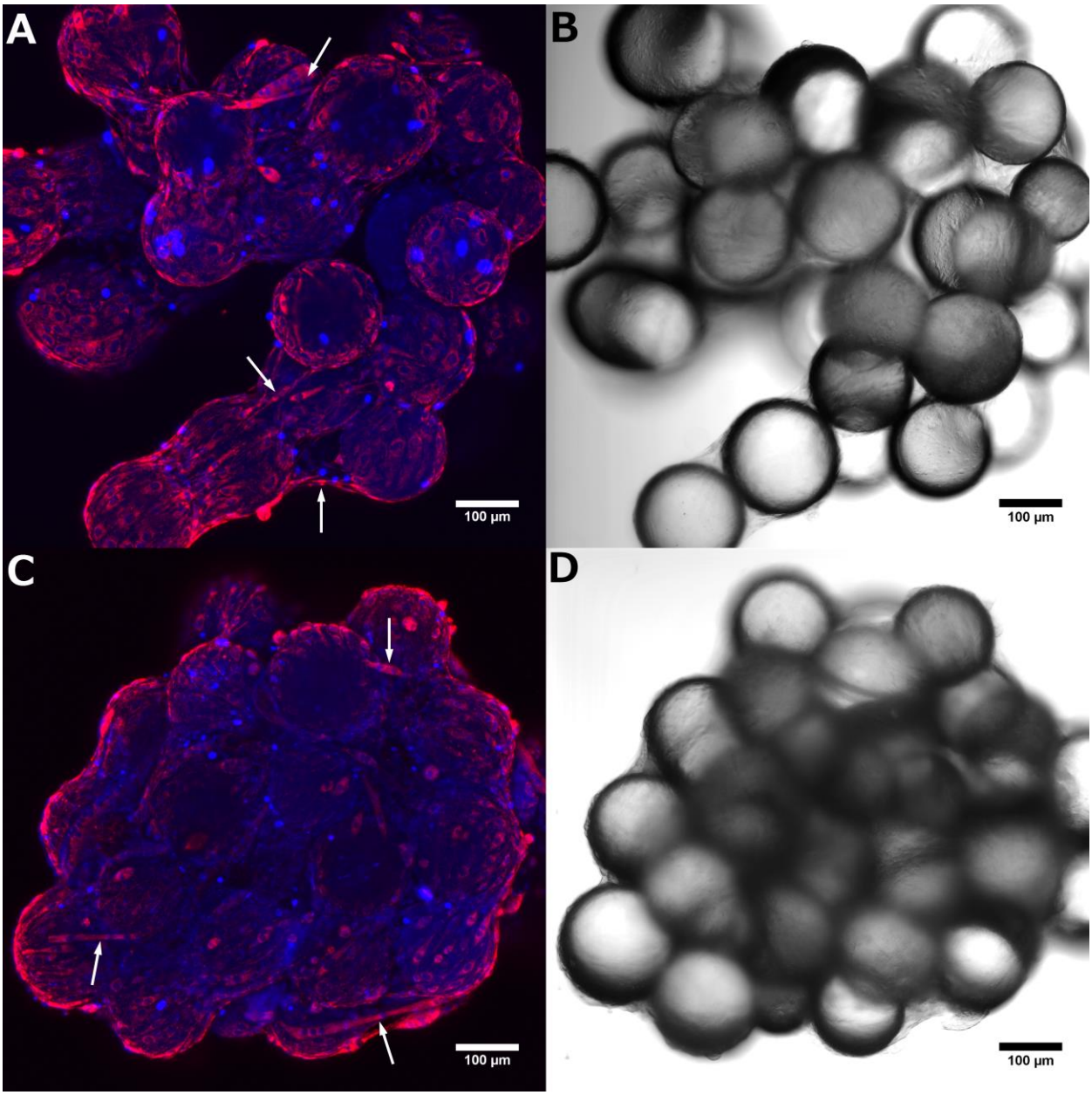

Figure 22. Microcarrier bead clusters after 15 days of culture, imaged at 10x magnification. Nuclei are stained blue with Hoechst 33342. Mitochondria are stained red with MitoTracker CMX-Ros. Normal gravity (A, B) and simulated microgravity (C, D) bead clusters both have differentiated, multi-nucleated myotubes spanning across bead gaps (white arrows). Scale bar = 100 µm.

Alginate Substrate Structure & Cell Morphology

Undifferentiated cells encapsulated in alginate were evenly distributed throughout the bead (Figure 23A), where encapsulation of differentiated cells resulted in irregular sheets with uneven distribution (Figure 23B). A section of an alginate bead containing differentiated cells reveals the encapsulation process forces the harvested muscle fibers into atypical configurations (Figure 23C), compared to the regular, parallel orientation common in standard tissue culture flasks (Figure 23D). For cells encapsulated in their undifferentiated state, minimal differentiation was observed after 15 days of culture. No differences in cell morphology were observed between the RCCS and normal gravity controls. Alginate bead degradation was minimal, as more than 90% of the beads were intact when they were harvested at the end of the culture period.

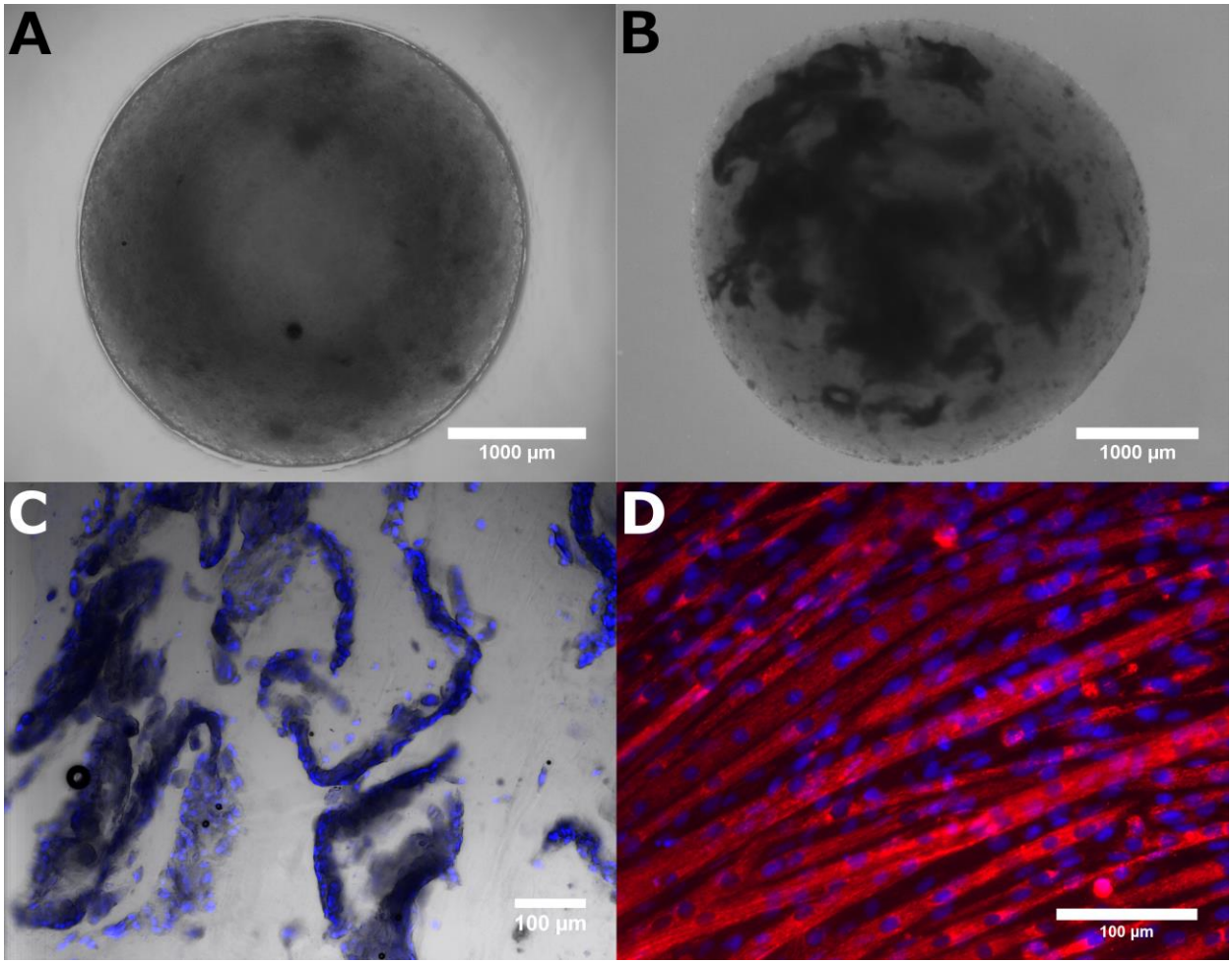

Figure 23. Alginate encapsulated undifferentiated (A) and differentiated cells (B) imaged at 2x magnification, scale bar = 1000 µm. Interior morphology of encapsulated differentiated cells in a 30 µm **s**ection of an alginate bead (C) compared to a standard T25 (D), scale bar = 100 µm. Nuclei are stained blue with Hoechst 33342 (C & D). Mitochondria are stained red with MitoTracker CMX-Ros (D only).

Atrophy Marker Expression

Alginate-encapsulated differentiated cells in the RCCS expressed significantly more MuRF1 than those in T25s, but the difference in MAFbx and Caspase 3 expression was not significant (Figure 24). Encapsulated undifferentiated cells in the RCCS expressed significantly

less MuRF1, MAFbx, and Caspase 3 than those in T25s, contrary to the hypothesized response (Figure 24).

When cultured on microcarriers, expression of MuRF1 and Caspase 3 was significantly elevated after 12 days in ULA T25s, followed by 3 days in the RCCS, relative to ULA T25 control flasks (Figure 24). Cultures that remained in the RCCS for 15 days also expressed significantly more MuRF1 and Caspase 3 than the ULA T25 control. The change in MAFbx was not significant for either simulated microgravity culture method but was larger for the ULA T25 (12 days) + RCCS (3 days) condition ($p=0.1$). Significance for all comparisons is detailed in Table 3.

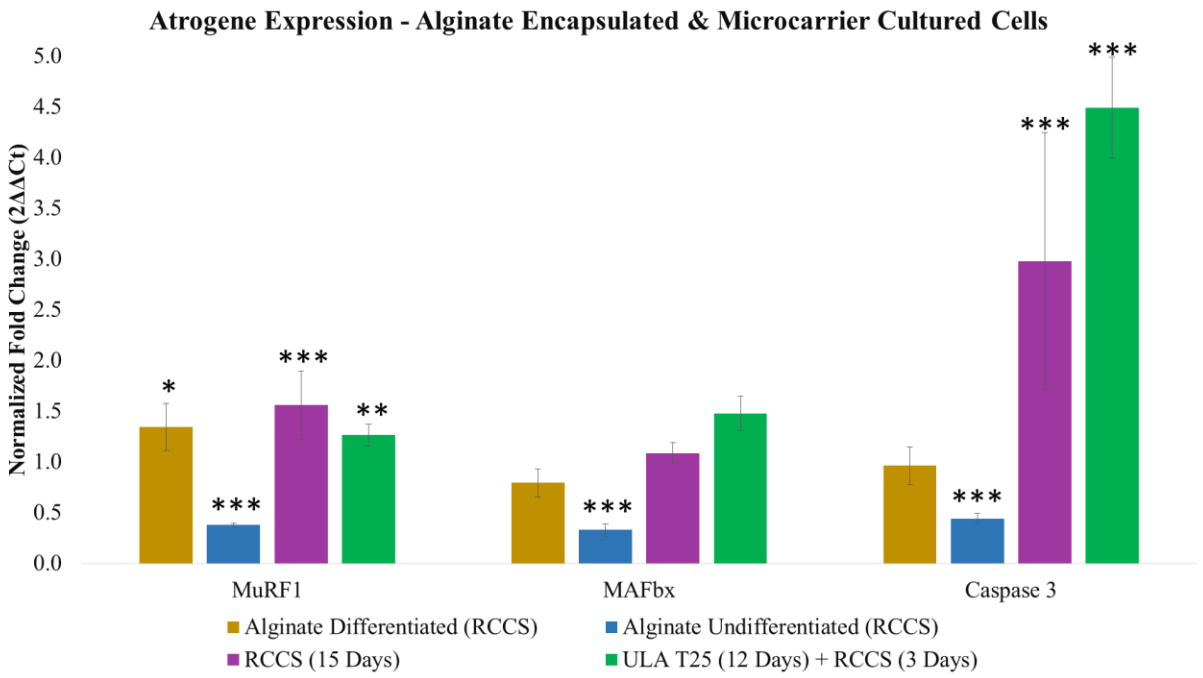

Figure 24 Average ± s.d. fold change in expression of mRNAs for alginate and microcarrier cultures, relative to their respective normal gravity controls (alginate N=4, microcarrier N=20) and normalized by GAPDH. * $p<0.05$, ** $p<0.01$, *** $p<0.001$. No marker = not significant. N=4 (alginate differentiated), N=4 (alginate undifferentiated), N=16 (RCCS), and N=8 (ULA T25 + RCCS). All replicates are biological replicates and significance was determined by *t*-test.

Table 3. Significance of microcarrier culture mRNA expression changes, as determined by Student's t-test. N=20 for ULA T25, N=16 for RCCS, N=8 for ULA T25 + RCCS, and N=4 for Horizontal RCCS. ns = not significant, * $p<0.05$, ** $p<0.01$, *** $p<0.001$. All replicates are biological replicates.

MuRF1	ULA T25	RCCS	Horiz. RCCS	ULA T25 + RCCS
ULA T25	—	***	***	**
RCCS	***	—	ns	**
Horiz. RCCS	***	ns	—	***
ULA T25 + RCCS	**	**	***	—

MAFbx	ULA T25	RCCS	Horiz. RCCS	ULA T25 + RCCS
ULA T25	—	ns	ns	ns
RCCS	ns	—	**	***
Horiz. RCCS	ns	**	—	***
ULA T25 + RCCS	ns	***	***	—

Caspase 3	ULA T25	RCCS	Horiz. RCCS	ULA T25 + RCCS
ULA T25	—	***	***	***
RCCS	***	—	ns	ns
Horiz. RCCS	***	ns	—	*
ULA T25 + RCCS	***	ns	*	—

Cells cultured in the RCCS for 15 days and those cultured in the RCCS for only 3 days following 12 days in ULA T25's had similarly significant increases in the key atrophy markers MuRF1 and Caspase 3. Due to shorter duration of RCCS culture, using the latter method allows for higher throughput testing in a given timeframe, as subsequent cultures need only be staggered by 3 days instead of 15. Therefore, the ULAT25 + RCCS method was selected for further development of the model and evaluation of Akt2, mTOR, Ankrd1, and Foxo3. Akt2, mTOR, and Foxo3 increased significantly in simulated microgravity, but the change in Ankrd1 was not significant (Figure 25).

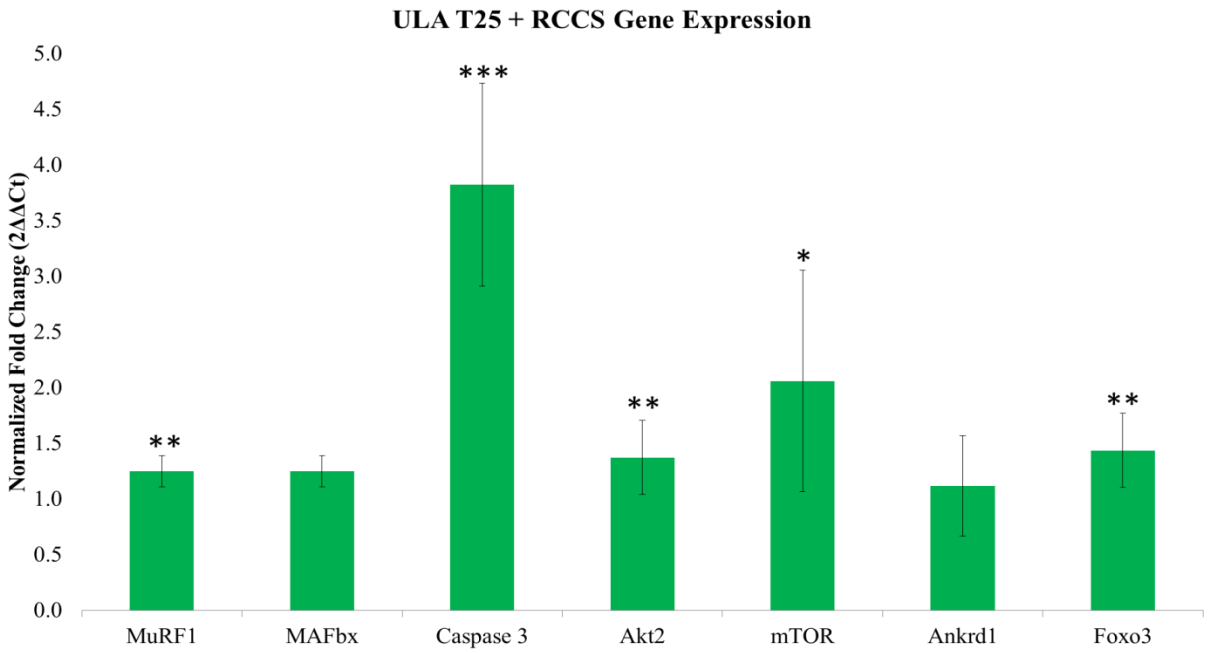

Figure 25. Average ± s.d. fold change in expression of mRNAs for ULA T25 + RCCS simulated microgravity cultures (N=8) relative to ULA T25 normal gravity control (N=20) and normalized by GAPDH. * $p<0.05$, ** $p<0.01$, *** $p<0.001$. All replicates are biological replicates and significance was determined by *t*-test. Change in MAFbx and Ankrd1 not significant.

Protein Concentration

Myosin heavy chain 4 (Myh4) was used to assess the extent of terminal differentiation. After 15 days of culture on microcarriers in ULA normal gravity control flasks, Myh4 concentration was 1.22±0.26 ng μg^{-1} total protein. Cells cultured in the RCCS for the final 3 days following 12 days in the ULA flasks had an Myh4 concentration of 2.13±0.48 ng μg^{-1} total protein. The difference between the normal gravity and simulated microgravity conditions was significant ($p<0.05$, N=4).

Discussion

We hypothesized that alginate encapsulated cells would exhibit more significant increases in atrophy marker expression than cells cultured on microcarriers, since an encapsulated three-dimensional mass of differentiated muscle tissue may exhibit greater inherent similarity to animal models than monolayers on the exterior of microcarriers. However, the alginate-encapsulated differentiated cells only exhibited an increase in MuRF1. Further, encapsulated undifferentiated cells had significantly lower expression of MuRF1, MAFbx, and Caspase 3 in simulated microgravity, which was the opposite of expected results (Figure 24). Low expression of atrophy markers for encapsulated undifferentiated cells may be due to insufficient myotube formation. The solid alginate structure limits cell-cell contact and morphology remained consistent over the 15 day culture period (Figure 23A). On the other hand, C2C12 cells cultured on polystyrene microcarrier beads for 12 days in ULA T25 flasks followed by 3 days in the RCCS significantly ($p<0.05$) express more MuRF1, Caspase 3, Akt2, mTOR, and Foxo3 than the normal gravity control of cells cultured in static ULA T25s for all 15 days, highlighting the early upregulation of these markers in simulated microgravity (Figure 24).

The timing of maximum MAFbx and MuRF1 expression has *in vivo* remains under investigation. Elevated expression has been reported at 3 days, 7 days, and 6 weeks, though differences in animal line and immobilization methods may be responsible[42, 44, 45]. Unlike MAFbx and MuRF1, *in vivo* atrophy models produce consistent significant increases in Caspase 3 over 5, 10, and 14 days[40, 41]. Our results *in vitro* indicate that MuRF1 expression is higher in cells cultured for 15 days in the RCCS, compared to 3 days in the RCCS after 12 days in ULA flasks, while Caspase 3 expression does not change significantly (Figure 24 & Table 3). We did not observe a significant change in MAFbx at either 3 or 15 days in simulated microgravity,

suggesting that the timing of upregulation differs from its partner E3 ligase MuRF1. In addition to the uncertain timing of peak upregulation, this discrepancy in MuRF1 and MAFbx upregulation may be due to the different roles of the two ligases. While MuRF1 and MAFbx both play an important part in the ubiquitin proteasome system, MuRF1 is more closely associated with degradation of myofibers, where MAFbx attenuates new protein synthesis and is not correlated with atrophy in every case[122, 123].

Increased expression of Akt2 and higher Myh4 concentrations in simulated microgravity indicate a higher percentage of differentiated cells compared to the normal gravity controls. mTOR, expected to be lower in simulated microgravity, instead increased significantly after 3 days in the RCCS (Figure 25). Additionally, while Foxo3 will activate MAFbx, Foxo3 was significantly upregulated while MAFbx—responsible for attenuating protein synthesis—was not (Figure 25) [107, 122]. Taken together, these results indicate that while the cells in simulated microgravity were undergoing atrophy—indicated by MuRF1, Caspase 3, and Foxo3—mTOR mediated protein synthesis and formation of new myotubes had not yet ceased.

Compared to *in vivo* methods, including casting, tenotomy, and hind limb unloading, our *in vitro* model resulted in a similar fold change in Caspase 3 and lower but still statistically significant increases in MuRF1 and Foxo3 (Table 4). While Caspase 3 is most strongly upregulated, apoptosis from shear forces is not likely due to the low shear environment of the RCCS[54]. The fold increase in MuRF1 after 12 days in normal gravity and 3 days in the RCCS was closer to that of 3 days post-tenotomy rather than 3 days post-immobilization via casting (Table 4). The *in vitro* model did not significantly increase MAFbx, but again the fold change was closer to that following tenotomy. In contrast to the large increase in Ankrd1 seen *in vivo*,

our *in vitro* model did not produce any significant changes (Table 4). While Ankrd1 is expressed in C2C12 cells, it was not significantly upregulated in this model[124, 125].

Table 4. Fold change in gene expression of atrophy-indicating mRNAs from this *in vitro* study (ULA T25 12 days + RCCS 3 days) compared to referenced work *in vivo*, as measured by qPCR. ns = not significant, ** $p<0.01$, *** $p<0.001$.

	In Vitro	*In Vivo*	*In Vivo* method
MuRF1	1.3^{**}	1.9, 1.6[45]	Casting 3 days, tenotomy 3 days
MAFbx	1.3^{ns}	2.7, 1.5[45]	Casting 3 days, tenotomy 3 days
Caspase 3	3.8^{***}	1.0, 3.3[45]	Casting 3 days, tenotomy 3 days
Ankrd1	1.1^{ns}	3.9[106]	Hind limb unloading 6 days
Foxo3	1.4^{**}	1.6[106]	Hind limb unloading 6 days

Turning the RCCS horizontal was investigated as a normal gravity control to account for the effects vessel geometry and fluid motion not present in static ULA tissue culture flasks. Despite these benefits, the horizontal RCCS was an ideal control due to significant differences in microcarrier bead cluster morphology and higher MuRF1 expression levels compared with the simulated microgravity conditions (RCCS, ULA T25 + RCCS) (not shown). Additionally, microcarrier beads in the horizontal RCCS adhered to the silicone gas transfer membrane, resulting in large sheets of cells not representative of the bead clusters in Figure 22. Shear forces from fluid motion in the RCCS are minimal and selecting a control with similar cluster morphology and consistently significant differences in mRNA expression is preferred[54].

Microcarrier beads and alginate encapsulation each have advantages and disadvantages in maximizing similarity with *in vivo* hind limb unloading methods. The advantages of microcarriers include ease of handling, live cell fluorescent imaging capability, and most importantly, that they support atrophy marker changes in C2C12 cells. Culture procedures with

microcarrier beads are simpler and more rapid than alginate encapsulation. The small size of the beads allows them to be transferred between containers via pipette. Harvest of RNA can be accomplished by adding the cell-covered microcarriers directly to the lysis buffer, reducing process time and opportunity for RNase activity. Most critically, simulated microgravity culture of C2C12 cells on microcarriers resulted in significant expression changes in multiple atrophy markers compared to the normal gravity control (Figure 25). However, MAFbx and Ankrd1 were not significantly upregulated and the fold increase in MuRF1 and Foxo3 were low, indicating that this model is incomplete when compared to atrophy modeling *in vivo* (Table 4).

Microcarriers carry some additional disadvantages regarding the culture method and morphology. The monolayer of tissue that forms over the bead surfaces does not replicate three-dimensional mature tissue *in vivo*. Compared to astronauts that begin with differentiated muscle tissue, microcarriers are first seeded with undifferentiated myoblasts which form multi-nucleated myotubes during culture. Despite this difference, the model remains clinically relevant as fusion and differentiation of muscle cells are important parts of myogenesis in adults[126]. Another disadvantage of microcarriers is the large variations in cluster diameter relative to alginate beads (Table 2). As settling rate within the RCCS varies with substrate diameter, a portion of the microcarrier clusters will not be maintained at the optimal settling rate to simulate microgravity. Additionally, bead cluster size increases over time, requiring daily monitoring and RPM adjustment.

While alginate did not support the desired changes in atrophy marker expression, it offers some beneficial properties compared to microcarriers. Alginate encapsulation of differentiated cells in a three-dimensional conformation improves morphological biosimilarity to mature tissue. However, the current implementation resulted in muscle fiber conformations not typical *in vivo*

(Figure 23C). Encapsulation also protects cells from exposure to mechanical stress within the RCCS. Fluid flow in the RCCS is designed to provide a low shear environment[54]. Still, cells experience mechanical stress from collisions of suspended substrates due to the rotation of the system. While cells encapsulated in alginate are protected from direct contact, the exposed nature of cells cultured on microcarriers means that collisions between beads will result in a direct impact to the cells. Furthermore, alginate beads have a more consistent size than microcarrier bead clusters and did not display the same variations in settling rate or require changes in the RCCS' RPM (Table 2).

The downsides of alginate, in addition to the lack of significant changes in atrophy marker expression, stem from their density, size, and opacity. While the solid structure of alginate protects cells from mechanical stress, it also limits the spreading of encapsulated cells, preventing formation of intercellular junctions necessary for myoblast fusion (Figure 23A). In contrast to the small and easy to handle microcarriers, alginate beads, with a diameter of 3252±103 μm, were too large to be aspirated into a pipette. Smaller alginate beads can be formed by using a higher gauge needle, but narrower needles were clogged by the large sheets of differentiated muscle tissue seen in Figure 23B. The large bead size also complicated imaging due to the opacity of alginate, which scattered too much light to allow fluorescent imaging of the interior without fixation and sectioning. While these issues are addressable with process modifications, the most significant issue is that nutrient and waste diffusion rates are dependent on depth, such that beads with tissues closer to the surface may behave differently than those with tissues encapsulated in the center. As the position of tissues within the bead is random, we attribute some of the variability in encapsulated differentiated samples to uneven distribution of tissues within the alginate beads.

Overall, culturing with microcarrier beads provides a better platform than alginate encapsulation for modeling muscular atrophy in C2C12 cells, though this model does not completely mimic the mRNA changes seen *in vivo*. Cultures on microcarrier beads resulted in irregular clusters covered with a monolayer of cells and sporadic myotubes (Figure 22) and appropriate atrophy marker expression to mimic *in vivo* studies only with regard to MuRF1, Caspase 3, and Foxo3, albeit with lower—but still significant—fold changes for MuRF1 and Foxo3 (Table 4). On the other hand, cultures with encapsulated cells resulted in static, regularly dispersed undifferentiated cells (Figure 23A) or unevenly dispersed sheets of differentiated tissue (Figure 23B) without consistent increases in expression of the selected atrophy markers. Therefore, we conclude that an *in vitro* model of microgravity-induced muscle atrophy using polystyrene microcarrier beads is superior to alginate encapsulation for cultured C2C12 cells, but not sufficient to mimic all of the select atrophy markers as in animal studies. Of the culture methods evaluated, the most significant and consistent increase in the selected atrophy markers, relative to GAPDH (Figure 25) was achieved with microcarriers cultured in static ULA flasks for 12 days, then moved to the RCCS for the final 3 days.

Our verification that the RCCS can produce increases in atrophy-specific mRNAs in cultured muscle cells is an important step towards completing a comprehensive ground-based *in vitro* model for spaceflight atrophy. Due to the lower number of atrophy markers upregulated and the lower fold changes in expression, relative to animal models, we believe the standard commercially available RCCS is not sufficient for use *in vitro* atrophy modeling and it does not match results *in vivo*. Nevertheless, our results *in vitro* are highly significant for MuRF1 ($p<0.01$), Foxo3 ($p<0.01$), and Caspase 3 ($p<0.001$), indicating that with further development, simulated microgravity systems may present a promising platform for investigation of atrophy

pathways and first-step design and selection of novel therapeutics necessary to ensure astronaut health and fitness during long-term spaceflight.

CHAPTER 6

CLOSING REMARKS

Overall, culturing with microcarrier beads provides a better platform for modeling microgravity-induced muscular atrophy with C2C12 cells than alginate encapsulation. Cultures on microcarrier beads resulted in irregular clusters covered with a monolayer of cells and sporadic myotubes, but allowed for ease of handling and, most importantly, resulted in appropriate atrophy marker expression to mimic hind limb unloading studies with regard to several key markers. On the other hand, cultures with encapsulated cells resulted in static, regularly dispersed undifferentiated cells or unevenly dispersed sheets of differentiated tissue without consistent increases in expression of the selected atrophy markers. Therefore, we conclude that an *in vitro* model of microgravity-induced muscle atrophy using polystyrene microcarrier beads is superior to alginate encapsulation for cultured C2C12 cells. To induce the most significant and consistent increase in these same atrophy markers, relative to GAPDH, a normal gravity control with microcarriers in static ULA flasks should be cultured for 15 days and compared with microcarriers cultured for 12 days in the same flasks, then moved to the RCCS for the final 3 days.

Due to variations in microcarrier bead cluster size, not all of the cells are maintained at the optimal settling rate to simulate microgravity. Despite the presence of such variations, C2C12 cells cultured on microcarriers in the RCCS for 3 days expressed significantly more

MuRF1, MAFbx, and caspase-3 than normal gravity controls. Alginate beads, having a more consistent size, did not display the same variations in settling rate. However, neither undifferentiated nor differentiated cells expressed significant increases in all three mRNA markers.

The verification that the RCCS can partially model atrophic conditions in cultured muscle cells is an important step towards completing a comprehensive ground-based *in vitro* model for spaceflight atrophy. Our ongoing work focuses on evaluating the effectiveness of antioxidants in attenuating the increase in MuRF1, MAFbx, and Caspase 3 seen with C2C12 cells cultured in simulated microgravity on microcarriers. We are also investigating adding radiation to more accurately simulate spaceflight conditions. The simulated microgravity model described herein produces increases in the same mRNA markers of muscular atrophy as *in vivo* hind limb unloading models, presenting a promising system for investigation of atrophy pathways and first-step design and selection of novel therapeutics necessary to ensure astronaut health and fitness during long-term spaceflight. Further development of the model with additional cell types, optimized encapsulation and additional microcarrier materials could improve biosimilarity. Combined with PCR arrays targeting a large number of genes, the model presented herein can help elucidate the mechanisms of action for atrophy countermeasures, providing a foundation for design and selection of novel therapeutics.

REFERENCES

[1] "66a89946869501.5607e7b32f730.png (600×450)," https://mir-s3-cdn-cf.behance.net/project_modules/disp/66a89946869501.5607e7b32f730.png.

[2] G. Clément: "The Musculo-Skeletal System in Space." Fundamentals of Space Medicine. pp. 181–216. *Springer New York* (2011).

[3] D. Williams, A. Kuipers, C. Mukai, and R. Thirsk: "Acclimation during space flight: effects on human physiology." *Can. Med. Assoc. J.* vol. 180, no. 13, pp. 1317–1323, 2009.

[4] G.R. Adams, V.J. Caiozzo, and K.M. Baldwin: "Skeletal muscle unweighting: spaceflight and ground-based models." *J. Appl. Physiol.* vol. 95, no. 6, pp. 2185–2201, 2003.

[5] L.C. Shackelford: "Musculoskeletal Response to Space Flight." In: M.D.,M.S, A. and P.M.R.B. and M.D, C.S.L.P. (eds.) Principles of Clinical Medicine for Space Flight. pp. 293–306. *Springer New York* (2008).

[6] P.E. Di Prampero, M.V. Narici, and P.A. Tesch: "Muscles in space." *World Gravity Res. Space Health Ind. Process. Paris Fr. Eur. Space Agency*. pp. 69–82, 2001.

[7] S.K. Powers, A.J. Smuder, and D.S. Criswell: "Mechanistic links between oxidative stress and disuse muscle atrophy." *Antioxid. Redox Signal.* vol. 15, no. 9, pp. 2519–2528, 2011.

[8] S. Trappe, D. Costill, P. Gallagher, A. Creer, J.R. Peters, H. Evans, D.A. Riley, and R.H. Fitts: "Exercise in space: human skeletal muscle after 6 months aboard the International Space Station." *J. Appl. Physiol.* vol. 106, no. 4, pp. 1159–1168, 2009.

[9] L. A, R. R, S. V, E. H, and H. T: "Regional muscle loss after short duration spaceflight." *Aviat. Space Environ. Med.* vol. 66, no. 12, pp. 1151–1154, 1995.

[10] M.A. Perhonen, F. Franco, L.D. Lane, J.C. Buckey, C.G. Blomqvist, J.E. Zerwekh, R.M. Peshock, P.T. Weatherall, and B.D. Levine: "Cardiac atrophy after bed rest and spaceflight." *J. Appl. Physiol. Bethesda Md 1985*. vol. 91, no. 2, pp. 645–653, 2001.

[11] S.H. Lecker, A.L. Goldberg, and W.E. Mitch: "Protein degradation by the ubiquitin–proteasome pathway in normal and disease states." *J. Am. Soc. Nephrol.* vol. 17, no. 7, pp. 1807–1819, 2006.

[12] S.C. Bodine, E. Latres, S. Baumhueter, V.K.-M. Lai, L. Nunez, B.A. Clarke, W.T. Poueymirou, F.J. Panaro, E. Na, K. Dharmarajan, Z.-Q. Pan, D.M. Valenzuela, T.M. DeChiara, T.N. Stitt, G.D. Yancopoulos, and D.J. Glass: "Identification of Ubiquitin Ligases Required for Skeletal Muscle Atrophy." *Science*. vol. 294, no. 5547, pp. 1704–1708, 2001.

[13] S.C. Bodine and L.M. Baehr: "Skeletal muscle atrophy and the E3 ubiquitin ligases MuRF1 and MAFbx/atrogin-1." *Am. J. Physiol.-Endocrinol. Metab.* vol. 307, no. 6, pp. E469–E484, 2014.

[14] E. Edström, M. Altun, M. Hägglund, and B. Ulfhake: "Atrogin-1/MAFbx and MuRF1 are downregulated in aging-related loss of skeletal muscle." *J. Gerontol. A. Biol. Sci. Med. Sci.* vol. 61, no. 7, pp. 663–674, 2006.

[15] S. Servais, D. Letexier, R. Favier, C. Duchamp, and D. Desplanches: "Prevention of unloading-induced atrophy by vitamin E supplementation: Links between oxidative stress and soleus muscle proteolysis?" *Free Radic. Biol. Med.* vol. 42, no. 5, pp. 627–635, 2007.

[16] E. Moran, F. Carbone, V. Augusti, F. Patrone, A. Ballestrero, and A. Nencioni: "Proteasome inhibitors as immunosuppressants: biological rationale and clinical experience." *Semin. Hematol.* vol. 49, no. 3, pp. 270–276, 2012.

[17] P. Fernando, J.F. Kelly, K. Balazsi, R.S. Slack, and L.A. Megeney: "Caspase 3 activity is required for skeletal muscle differentiation." *Proc. Natl. Acad. Sci.* vol. 99, no. 17, pp. 11025–11030, 2002.

[18] S.K. Powers, A.N. Kavazis, and K.C. DeRuisseau: "Mechanisms of disuse muscle atrophy: role of oxidative stress." *Am. J. Physiol. Regul. Integr. Comp. Physiol.* vol. 288, no. 2, pp. R337-344, 2005.

[19] E. Cabiscol, J. Tamarit, and J. Ros: “Oxidative stress in bacteria and protein damage by reactive oxygen species.” *Int. Microbiol.* vol. 3, no. 1, pp. 3–8, 2010.

[20] F.A. Cucinotta and M. Durante: “Cancer risk from exposure to galactic cosmic rays: implications for space exploration by human beings.” *Lancet Oncol.* vol. 7, no. 5, pp. 431–435, 2006.

[21] E.L. Alpen, P. Powers-Risius, S.B. Curtis, and R. DeGuzman: “Tumorigenic Potential of High-Z, High-LET Charged-Particle Radiations.” *Radiat. Res.* vol. 136, no. 3, pp. 382–391, 1993.

[22] F.A. Cucinotta: “Space Radiation Risks for Astronauts on Multiple International Space Station Missions.” *PLOS ONE*. vol. 9, no. 4, pp. e96099, 2014.

[23] P.K. Datta, J.E. Moulder, B.L. Fish, E.P. Cohen, and E.A. Lianos: “Induction of heme oxygenase 1 in radiation nephropathy: role of angiotensin II.” *Radiat. Res.* vol. 155, no. 5, pp. 734–739, 2001.

[24] M. Giriş, Y. Erbil, S. Oztezcan, V. Olgaç, U. Barbaros, U. Deveci, B. Kirgiz, M. Uysal, and G.A. Toker: “The effect of heme oxygenase-1 induction by glutamine on radiation-induced intestinal damage: the effect of heme oxygenase-1 on radiation enteritis.” *Am. J. Surg.* vol. 191, no. 4, pp. 503–509, 2006.

[25] M.D. Maines: “The heme oxygenase system: a regulator of second messenger gases.” *Annu. Rev. Pharmacol. Toxicol.* vol. 37, pp. 517–554, 1997.

[26] S. Zhang, C. Song, J. Zhou, L. Xie, X. Meng, P. Liu, J. Cao, X. Zhang, W.-Q. Ding, and J. Wu: “Amelioration of radiation-induced skin injury by adenovirus-mediated heme oxygenase-1 (HO-1) overexpression in rats.” *Radiat. Oncol. Lond. Engl.* vol. 7, pp. 4, 2012.

[27] S. Servais, D. Letexier, R. Favier, C. Duchamp, and D. Desplanches: “Prevention of unloading-induced atrophy by vitamin E supplementation: links between oxidative stress and soleus muscle proteolysis?” *Free Radic. Biol. Med.* vol. 42, no. 5, pp. 627–635, 2007.

[28] A. Hj, D. Ja, and S. Jm: “Supplementation of vitamin E may attenuate skeletal muscle immobilization atrophy.” *Int. J. Sports Med.* vol. 18, no. 3, pp. 157–160, 1997.

[29] B.J. Smith, E.A. Lucas, R.T. Turner, G.L. Evans, M.R. Lerner, D.J. Brackett, B.J. Stoecker, and B.H. Arjmandi: “Vitamin E Provides Protection for Bone in Mature Hindlimb Unloaded Male Rats.” *Calcif. Tissue Int.* vol. 76, no. 4, pp. 272–279, 2004.

[30] V.K. Singh, S.Y. Wise, O.O. Fatanmi, L.A. Beattie, E.J. Ducey, and T.M. Seed: “Alpha-tocopherol succinate- and AMD3100-mobilized progenitors mitigate radiation combined injury in mice.” *J. Radiat. Res. (Tokyo)*. vol. 55, no. 1, pp. 41–53, 2014.

[31] X.H. Li, C.T. Ha, D. Fu, M.R. Landauer, S.P. Ghosh, and M. Xiao: “Delta-Tocotrienol Suppresses Radiation-Induced MicroRNA-30 and Protects Mice and Human CD34+ Cells from Radiation Injury.” *PLOS ONE*. vol. 10, no. 3, pp. e0122258, 2015.

[32] C.M. Compadre, A. Singh, S. Thakkar, G. Zheng, P.J. Breen, S. Ghosh, M. Kiaei, M. Boerma, K.I. Varughese, and M. Hauer-Jensen: “Molecular Dynamics Guided Design of Tocoflexol: A New Radioprotectant Tocotrienol with Enhanced Bioavailability.” *Drug Dev. Res.* vol. 75, no. 1, pp. 10–22, 2014.

[33] E.R. Morey-Holton and R.K. Globus: “Hindlimb unloading rodent model: technical aspects.” *J. Appl. Physiol.* vol. 92, no. 4, pp. 1367–1377, 2002.

[34] V.C. Foletta, L.J. White, A.E. Larsen, B. Léger, and A.P. Russell: “The role and regulation of MAFbx/atrogin-1 and MuRF1 in skeletal muscle atrophy.” *Pflüg. Arch. - Eur. J. Physiol.* vol. 461, no. 3, pp. 325–335, 2011.

[35] S. Labeit, C.H. Kohl, C.C. Witt, D. Labeit, J. Jung, and H. Granzier: “Modulation of muscle atrophy, fatigue and MLC phosphorylation by MuRF1 as indicated by hindlimb suspension studies on MuRF1-KO mice.” *BioMed Res. Int.* vol. 2010, 2010.

[36] W.O. Kline, F.J. Panaro, H. Yang, and S.C. Bodine: “Rapamycin inhibits the growth and muscle-sparing effects of clenbuterol.” *J. Appl. Physiol.* vol. 102, no. 2, pp. 740–747, 2007.

[37] F. Haddad, G.R. Adams, P.W. Bodell, and K.M. Baldwin: “Isometric resistance exercise fails to counteract skeletal muscle atrophy processes during the initial stages of unloading.” *J. Appl. Physiol.* vol. 100, no. 2, pp. 433–441, 2006.

[38] T. Maki, D. Yamamoto, S. Nakanishi, K. Iida, G. Iguchi, Y. Takahashi, H. Kaji, K. Chihara, and Y. Okimura: “Branched-chain amino acids reduce hindlimb suspension-induced muscle atrophy and protein levels of atrogin-1 and MuRF1 in rats.” *Nutr. Res.* vol. 32, no. 9, pp. 676–683, 2012.

[39] D.L. Allen, E.R. Bandstra, B.C. Harrison, S. Thorng, L.S. Stodieck, P.J. Kostenuik, S. Morony, D.L. Lacey, T.G. Hammond, L.L. Leinwand, W.S. Argraves, T.A. Bateman, and J.L. Barth: “Effects of spaceflight on murine skeletal muscle gene expression.” *J. Appl. Physiol.* vol. 106, no. 2, pp. 582–595, 2009.

[40] P. Berthon, S. Duguez, F.B. Favier, A. Amirouche, L. Feasson, L. Vico, C. Denis, and D. Freyssenet: “Regulation of ubiquitin–proteasome system, caspase enzyme activities, and extracellular proteinases in rat soleus muscle in response to unloading.” *Pflüg. Arch.-Eur. J. Physiol.* vol. 454, no. 4, pp. 625–633, 2007.

[41] H. Fujino, A. Ishihara, S. Murakami, T. Yasuhara, H. Kondo, S. Mohri, I. Takeda, and R.R. Roy: “Protective effects of exercise preconditioning on hindlimb unloading-induced atrophy of rat soleus muscle.” *Acta Physiol.* vol. 197, no. 1, pp. 65–74, 2009.

[42] S. Al-Nassan, N. Fujita, H. Kondo, S. Murakami, and H. Fujino: “Chronic exercise training down-regulates TNF-α and atrogin-1/MAFbx in mouse gastrocnemius muscle atrophy induced by hindlimb unloading.” *Acta Histochem. Cytochem.* vol. 45, no. 6, pp. 343–349, 2012.

[43] T. Okamoto, S. Torii, and S. Machida: “Differential gene expression of muscle-specific ubiquitin ligase MAFbx/Atrogin-1 and MuRF1 in response to immobilization-induced atrophy of slow-twitch and fast-twitch muscles.” *J. Physiol. Sci.* vol. 61, no. 6, pp. 537, 2011.

[44] E.J. Stevenson, P.G. Giresi, A. Koncarevic, and S.C. Kandarian: “Global analysis of gene expression patterns during disuse atrophy in rat skeletal muscle.” *J. Physiol.* vol. 551, no. 1, pp. 33–48, 2003.

[45] P. Bialek, C. Morris, J. Parkington, M. St. Andre, J. Owens, P. Yaworsky, H. Seeherman, and S.A. Jelinsky: “Distinct protein degradation profiles are induced by different disuse models of skeletal muscle atrophy.” *Physiol. Genomics*. vol. 43, no. 19, pp. 1075–1086, 2011.

[46] J. Evans, G.M. Mulenburg, J.S. Harper, T.L. Skundberg, M. Navidi, and S.B. Arnaud: “A metabolic cage for the hindlimb suspended rat.” 1994.

[47] S.A. Lloyd, E.R. Bandstra, J.S. Willey, S.E. Riffle, L. Tirado-Lee, G.A. Nelson, M.J. Pecaut, and T.A. Bateman: “Effect of proton irradiation followed by hindlimb unloading on bone in mature mice: a model of long-duration spaceflight.” *Bone*. vol. 51, no. 4, pp. 756–764, 2012.

[48] X.W. Mao, N.C. Nishiyama, M. Campbell-Beachler, P. Gifford, K.E. Haynes, D.S. Gridley, and M.J. Pecaut: “Role of nadph oxidase as a mediator of oxidative damage in low-dose irradiated and hindlimb-unloaded mice.” *Radiat. Res.* vol. 188, no. 4, pp. 392–399, 2017.

[49] M. Xin, Y. Yang, D. Zhang, J. Wang, S. Chen, and D. Zhou: “Attenuation of hind-limb suspension-induced bone loss by curcumin is associated with reduced oxidative stress and increased vitamin D receptor expression.” *Osteoporos. Int.* vol. 26, no. 11, pp. 2665–2676, 2015.

[50] E. Morey-Holton, R.K. Globus, A. Kaplansky, and G. Durnova: “The hindlimb unloading rat model: literature overview, technique update and comparison with space flight data.” *Adv. Space Biol. Med.* vol. 10, pp. 7–40, 2005.

[51] F. Gaignier, V. Schenten, M.D.C. Bittencourt, G. Gauquelin-Koch, J.-P. Frippiat, and C. Legrand-Frossi: “Three weeks of murine hindlimb unloading induces shifts from B to T and from th to tc splenic lymphocytes in absence of stress and differentially reduces cell-specific mitogenic responses.” *PloS One*. vol. 9, no. 3, pp. e92664, 2014.

[52] C.A. Ray, M. Vasques, T.A. Miller, M.K. Wilkerson, and M.D. Delp: “Effect of short-term microgravity and long-term hindlimb unloading on rat cardiac mass and function.” *J. Appl. Physiol.* vol. 91, no. 3, pp. 1207–1213, 2001.

[53] H. Kondo, K. Yumoto, J.S. Alwood, R. Mojarrab, A. Wang, E.A. Almeida, N.D. Searby, C.L. Limoli, and R.K. Globus: “Oxidative stress and gamma radiation-induced cancellous bone loss with musculoskeletal disuse.” *J. Appl. Physiol.* vol. 108, no. 1, pp. 152–161, 2009.

[54] R.P. Schwarz, T.J. Goodwin, and D.A. Wolf: “Cell culture for three-dimensional modeling in rotating-wall vessels: an application of simulated microgravity.” *J. Tissue Cult. Methods Tissue Cult. Assoc. Man. Cell Tissue Organ Cult. Proced.* vol. 14, no. 2, pp. 51–57, 1992.

[55] S.L. Wuest, S. Richard, phane, S. Kopp, D. Grimm, and M. Egli: “Simulated Microgravity: Critical Review on the Use of Random Positioning Machines for Mammalian Cell Culture.” *BioMed Res. Int.* vol. 2015, pp. e971474, 2015.

[56] C.E. Torgan, S.S. Burge, A.M. Collinsworth, G.A. Truskey, and W.E. Kraus: “Differentiation of mammalian skeletal muscle cells cultured on microcarrier beads in a rotating cell culture system.” *Med. Biol. Eng. Comput.* vol. 38, no. 5, pp. 583–590, 2000.

[57] C. Girardi, C.D. Pittà, S. Casara, G. Sales, G. Lanfranchi, L. Celotti, and M. Mognato: “Analysis of miRNA and mRNA Expression Profiles Highlights Alterations in Ionizing Radiation Response of Human Lymphocytes under Modeled Microgravity.” *PLOS ONE*. vol. 7, no. 2, pp. e31293, 2012.

[58] J. Goyden, K. Tawara, D. Hedeen, J.S. Willey, J.T. Oxford, and C.L. Jorcyk: “The Effect of OSM on MC3T3-E1 Osteoblastic Cells in Simulated Microgravity with Radiation.” *PLOS ONE*. vol. 10, no. 6, pp. e0127230, 2015.

[59] G. Molnar, N.A. Schroedl, S.R. Gonda, and C.R. Hartzell: “Skeletal muscle satellite cells cultured in simulated microgravity.” *In Vitro Cell. Dev. Biol. Anim.* vol. 33, no. 5, pp. 386–391, 1997.

[60] D. Yaffe and O. Saxel: “Serial passaging and differentiation of myogenic cells isolated from dystrophic mouse muscle.” *Nature*. vol. 270, no. 5639, pp. 725–727, 1977.

[61] J.L. Drury and D.J. Mooney: “Hydrogels for tissue engineering: scaffold design variables and applications.” *Biomaterials*. vol. 24, no. 24, pp. 4337–4351, 2003.

[62] O. Smidsrød, G. Skja, and others: “Alginate as immobilization matrix for cells.” *Trends Biotechnol.* vol. 8, pp. 71–78, 1990.

[63] L. Baruch and M. Machluf: “Alginate–chitosan complex coacervation for cell encapsulation: Effect on mechanical properties and on long-term viability.” *Biopolymers*. vol. 82, no. 6, pp. 570–579, 2006.

[64] B. Irmanida, R. Devi, M. Kusdiantoro, and P. Wahono Esthi: “Leydig Cells Encapsulation with Alginate-Chitosan: Optimization of Microcapsule Formation.” *J. Encapsulation Adsorpt. Sci.* vol. 2012, 2012.

[65] S.K. Williams, J.S. Touroo, K.H. Church, and J.B. Hoying: “Encapsulation of Adipose Stromal Vascular Fraction Cells in Alginate Hydrogel Spheroids Using a Direct-Write Three-Dimensional Printing System.” *BioResearch Open Access*. vol. 2, no. 6, pp. 448–454, 2013.

[66] M. Peirone, C.J.D. Ross, G. Hortelano, J.L. Brash, and P.L. Chang: “Encapsulation of various recombinant mammalian cell types in different alginate microcapsules.” *J. Biomed. Mater. Res.* vol. 42, no. 4, pp. 587–596, 1998.

[67] N. Wang, G. Adams, L. Buttery, F.H. Falcone, and S. Stolnik: “Alginate encapsulation technology supports embryonic stem cells differentiation into insulin-producing cells.” *J. Biotechnol.* vol. 144, no. 4, pp. 304–312, 2009.

[68] C. Stabler, K. Wilks, A. Sambanis, and I. Constantinidis: “The effects of alginate composition on encapsulated βTC3 cells.” *Biomaterials*. vol. 22, no. 11, pp. 1301–1310, 2001.

[69] A.K.-L. Chen, S. Reuveny, and S.K.W. Oh: “Application of human mesenchymal and pluripotent stem cell microcarrier cultures in cellular therapy: Achievements and future direction.” *Biotechnol. Adv.* vol. 31, no. 7, pp. 1032–1046, 2013.

[70] S.M. Badenes, T.G. Fernandes, C.A.V. Rodrigues, M.M. Diogo, and J.M.S. Cabral: “Microcarrier-based platforms for in vitro expansion and differentiation of human pluripotent stem cells in bioreactor culture systems.” *J. Biotechnol.* vol. 234, pp. 71–82, 2016.

[71] C. Bardouille, J. Lehmann, P. Heimann, and H. Jockusch: “Growth and differentiation of permanent and secondary mouse myogenic cell lines on microcarriers.” *Appl. Microbiol. Biotechnol.* vol. 55, no. 5, pp. 556–562, 2001.

[72] R.E. Akins, N.A. Schroedl, S.R. Gonda, and C.R. Hartzell: “Neonatal rat heart cells cultured in simulated microgravity.” *Vitro Cell. Dev. Biol. - Anim.* vol. 33, no. 5, pp. 337–343, 1997.

[73] D.H. Slentz, G.A. Truskey, and W.E. Kraus: “Effects of chronic exposure to simulated microgravity on skeletal muscle cell proliferation and differentiation.” *In Vitro Cell. Dev. Biol. Anim.* vol. 37, no. 3, pp. 148–156, 2001.

[74] L. Goldstein and E.A. Newsholme: “The formation of alanine from amino acids in diaphragm muscle of the rat.” *Biochem. J.* vol. 154, no. 2, pp. 555–558, 1976.

[75] Y. Shimomura, T. Murakami, N. Nakai, M. Nagasaki, and R.A. Harris: “Exercise Promotes BCAA Catabolism: Effects of BCAA Supplementation on Skeletal Muscle during Exercise.” *J. Nutr.* vol. 134, no. 6, pp. 1583S-1587S, 2004.

[76] R.A. Kerr: “Planetary exploration. Radiation will make astronauts’ trip to Mars even riskier.” *Science*. vol. 340, no. 6136, pp. 1031, 2013.

[77] Bio-Rad Laboratories, Inc.: “General Protocol for Western Blotting.”

[78] E.P. Rogakou, D.R. Pilch, A.H. Orr, V.S. Ivanova, and W.M. Bonner: “DNA Double-stranded Breaks Induce Histone H2AX Phosphorylation on Serine 139.” *J. Biol. Chem.* vol. 273, no. 10, pp. 5858–5868, 1998.

[79] D.E. Barañano, M. Rao, C.D. Ferris, and S.H. Snyder: “Biliverdin reductase: A major physiologic cytoprotectant.” *Proc. Natl. Acad. Sci. U. S. A.* vol. 99, no. 25, pp. 16093, 2002.

[80] S.K. Powers, A.J. Smuder, and A.R. Judge: “Oxidative stress and disuse muscle atrophy: cause or consequence?” *Curr. Opin. Clin. Nutr. Metab. Care*. vol. 15, no. 3, pp. 240–245, 2012.

[81] T.P. Stein: “Space flight and oxidative stress.” *Nutr. Burbank Los Angel. Cty. Calif*. vol. 18, no. 10, pp. 867–871, 2002.

[82] J.M. Lawler, W. Song, and S.R. Demaree: “Hindlimb unloading increases oxidative stress and disrupts antioxidant capacity in skeletal muscle.” *Free Radic. Biol. Med.* vol. 35, no. 1, pp. 9–16, 2003.

[83] K. Min, A.J. Smuder, O.-S. Kwon, A.N. Kavazis, H.H. Szeto, and S.K. Powers: “Mitochondrial-targeted antioxidants protect skeletal muscle against immobilization-induced muscle atrophy.” *J. Appl. Physiol. Bethesda Md 1985*. vol. 111, no. 5, pp. 1459–1466, 2011.

[84] T. Ito, D. Chen, C.-W.T. Chang, T. Kenmochi, T. Saito, S. Suzuki, and J.Y. Takemoto: “Mesobiliverdin IXα Enhances Rat Pancreatic Islet Yield and Function.” *Front. Pharmacol.* vol. 4, pp. 50, 2013.

[85] A. Nakao, N. Murase, C. Ho, H. Toyokawa, T.R. Billiar, and S. Kanno: “Biliverdin administration prevents the formation of intimal hyperplasia induced by vascular injury.” *Circulation*. vol. 112, no. 4, pp. 587–591, 2005.

[86] S. Song, S. Wang, J. Ma, L. Yao, H. Xing, L. Zhang, L. Liao, and D. Zhu: “Biliverdin reductase/bilirubin mediates the anti-apoptotic effect of hypoxia in pulmonary arterial smooth muscle cells through ERK1/2 pathway.” *Exp. Cell Res.* vol. 319, no. 13, pp. 1973–1987, 2013.

[87] T. Jansen and A. Daiber: “Direct Antioxidant Properties of Bilirubin and Biliverdin. Is there a Role for Biliverdin Reductase?” *Front. Pharmacol.* vol. 3, pp. 30, 2012.

[88] C.-H. Park, T.-J. Ju, Y.-W. Kim, J.-M. Dan, J.-Y. Kim, Y.-D. Kim, J.-S. Seo, and S.-Y. Park: "Hemin, heme oxygenase-1 inducer, attenuates immobilization-induced skeletal muscle atrophy in mice." *Life Sci.* vol. 92, no. 12, pp. 740–746, 2013.

[89] M. Kozakowska, M. Ciesla, A. Stefanska, K. Skrzypek, H. Was, A. Jazwa, A. Grochot-Przeczek, J. Kotlinowski, A. Szymula, A. Bartelik, M. Mazan, O. Yagensky, U. Florczyk, K. Lemke, A. Zebzda, G. Dyduch, W. Nowak, K. Szade, J. Stepniewski, M. Majka, R. Derlacz, A. Loboda, J. Dulak, and A. Jozkowicz: "Heme oxygenase-1 inhibits myoblast differentiation by targeting myomirs." *Antioxid. Redox Signal.* vol. 16, no. 2, pp. 113–127, 2012.

[90] S. Trappe, D. Costill, P. Gallagher, A. Creer, J.R. Peters, H. Evans, D.A. Riley, and R.H. Fitts: "Exercise in space: human skeletal muscle after 6 months aboard the International Space Station." *J. Appl. Physiol. Bethesda Md 1985*. vol. 106, no. 4, pp. 1159–1168, 2009.

[91] B. Wegiel, C.J. Baty, D. Gallo, E. Csizmadia, J.R. Scott, A. Akhavan, B.Y. Chin, E. Kaczmarek, J. Alam, F.H. Bach, B.S. Zuckerbraun, and L.E. Otterbein: "Cell surface biliverdin reductase mediates biliverdin-induced anti-inflammatory effects via phosphatidylinositol 3-kinase and Akt." *J. Biol. Chem.* vol. 284, no. 32, pp. 21369–21378, 2009.

[92] M.L. Urso, A.G. Scrimgeour, Y.-W. Chen, P.D. Thompson, and P.M. Clarkson: "Analysis of human skeletal muscle after 48 h immobilization reveals alterations in mRNA and protein for extracellular matrix components." *J. Appl. Physiol.* vol. 101, no. 4, pp. 1136–1148, 2006.

[93] W. Qiu, B. Leibowitz, L. Zhang, and J. Yu: "Growth factors protect intestinal stem cells from radiation-induced apoptosis by suppressing PUMA through the PI3K/AKT/p53 axis." *Oncogene*. vol. 29, no. 11, pp. 1622–1632, 2010.

[94] Q. Gu, D. Wang, X. Wang, R. Peng, J. Liu, T. Jiang, Z. Wang, S. Wang, and H. Deng: "Basic Fibroblast Growth Factor Inhibits Radiation-Induced Apoptosis of HUVECs. I. The PI3K/AKT Pathway and Induction of Phosphorylation of BAD." *Radiat. Res.* vol. 161, no. 6, pp. 692–702, 2004.

[95] T. Matsui, J. Tao, F. del Monte, K.H. Lee, L. Li, M. Picard, T.L. Force, T.F. Franke, R.J. Hajjar, and A. Rosenzweig: "Akt activation preserves cardiac function and prevents injury after transient cardiac ischemia in vivo." *Circulation*. vol. 104, no. 3, pp. 330–335, 2001.

[96] T. Nagoshi, T. Matsui, T. Aoyama, A. Leri, P. Anversa, L. Li, W. Ogawa, F. del Monte, J.K. Gwathmey, L. Grazette, B.A. Hemmings, B. Hemmings, D.A. Kass, H.C. Champion, and A. Rosenzweig: "PI3K rescues the detrimental effects of chronic Akt activation in the heart during ischemia/reperfusion injury." *J. Clin. Invest.* vol. 115, no. 8, pp. 2128–2138, 2005.

[97] F.A. Wagener, A. Eggert, O.C. Boerman, W.J. Oyen, A. Verhofstad, N.G. Abraham, G. Adema, Y. van Kooyk, T. de Witte, and C.G. Figdor: "Heme is a potent inducer of inflammation in mice and is counteracted by heme oxygenase." *Blood*. vol. 98, no. 6, pp. 1802–1811, 2001.

[98] L. Gonzalez-Michaca, G. Farrugia, A.J. Croatt, J. Alam, and K.A. Nath: "Heme: a determinant of life and death in renal tubular epithelial cells." *Am. J. Physiol. Renal Physiol.* vol. 286, no. 2, pp. F370-377, 2004.

[99] S.J.S. Paul W Sylvester: "Mechanisms mediating the antiproliferative and apoptotic effects of vitamin E in mammary cancer cells." *Front. Biosci. J. Virtual Libr.* vol. 10, no. 1–3, pp. 699–709, 2005.

[100] B.B. Aggarwal, C. Sundaram, S. Prasad, and R. Kannappan: "Tocotrienols, the Vitamin E of the 21st Century: It's Potential Against Cancer and Other Chronic Diseases." *Biochem. Pharmacol.* vol. 80, no. 11, pp. 1613–1631, 2010.

[101] S.M. Senf, S.L. Dodd, J.M. McClung, and A.R. Judge: "Hsp70 overexpression inhibits NF-kappaB and Foxo3a transcriptional activities and prevents skeletal muscle atrophy." *FASEB J. Off. Publ. Fed. Am. Soc. Exp. Biol.* vol. 22, no. 11, pp. 3836–3845, 2008.

[102] K. Marimuthu, A.J. Murton, and P.L. Greenhaff: “Mechanisms regulating muscle mass during disuse atrophy and rehabilitation in humans.” *J. Appl. Physiol.* vol. 110, no. 2, pp. 555–560, 2010.
[103] M. Vandromme, A. Rochat, R. Meier, G. Carnac, D. Besser, B.A. Hemmings, A. Fernandez, and N.J. Lamb: “Protein kinase B β/Akt2 plays a specific role in muscle differentiation.” *J. Biol. Chem.* vol. 276, no. 11, pp. 8173–8179, 2001.
[104] P. Rotwein and E.M. Wilson: “Distinct actions of Akt1 and Akt2 in skeletal muscle differentiation.” *J. Cell. Physiol.* vol. 219, no. 2, pp. 503–511, 2009.
[105] M. Sandri, C. Sandri, A. Gilbert, C. Skurk, E. Calabria, A. Picard, K. Walsh, S. Schiaffino, S.H. Lecker, and A.L. Goldberg: “Foxo transcription factors induce the atrophy-related ubiquitin ligase atrogin-1 and cause skeletal muscle atrophy.” *Cell*. vol. 117, no. 3, pp. 399–412, 2004.
[106] C.-L. Wu, S.C. Kandarian, and R.W. Jackman: “Identification of Genes that Elicit Disuse Muscle Atrophy via the Transcription Factors p50 and Bcl-3.” *PLOS ONE*. vol. 6, no. 1, pp. e16171, 2011.
[107] J. Zhao, J.J. Brault, A. Schild, P. Cao, M. Sandri, S. Schiaffino, S.H. Lecker, and A.L. Goldberg: “FoxO3 coordinately activates protein degradation by the autophagic/lysosomal and proteasomal pathways in atrophying muscle cells.” *Cell Metab.* vol. 6, no. 6, pp. 472–483, 2007.
[108] M.-S. Yoon: “mTOR as a Key Regulator in Maintaining Skeletal Muscle Mass.” *Front. Physiol.* vol. 8, 2017.
[109] J. Zhao, B. Zhai, S.P. Gygi, and A.L. Goldberg: “mTOR inhibition activates overall protein degradation by the ubiquitin proteasome system as well as by autophagy.” *Proc. Natl. Acad. Sci.* vol. 112, no. 52, pp. 15790–15797, 2015.
[110] L. Laure, L. Suel, C. Roudaut, N. Bourg, A. Ouali, M. Bartoli, I. Richard, and N. Danièle: “Cardiac ankyrin repeat protein is a marker of skeletal muscle pathological remodelling.” *FEBS J.* vol. 276, no. 3, pp. 669–684, 2009.
[111] M.L. Marquette, D. Byerly, M. Sognier, and J.D. Sato: “The effects of three-dimensional cell culture on single myoblasts.” *Vitro Cell. Dev. Biol. - Anim.* vol. 44, no. 3 & 4, pp. 105–114, 2008.
[112] C.A. Pacak, M.-T. Eddy, L. Woodhull, K.-R. Wang, I. Alpatov, S. Fullen, R.P. Dowd, Y.-H. Choi, and D.B. Cowan: “Microcarrier-Based Expansion of Adult Murine Side Population Stem Cells.” *PLOS ONE*. vol. 8, no. 1, pp. e55187, 2013.
[113] M.L. Urso, A.G. Scrimgeour, Y.-W. Chen, P.D. Thompson, and P.M. Clarkson: “Analysis of human skeletal muscle after 48 h immobilization reveals alterations in mRNA and protein for extracellular matrix components.” *J. Appl. Physiol.* vol. 101, no. 4, pp. 1136–1148, 2006.
[114] K.A. Reardon, J. Davis, R.M. Kapsa, P. Choong, and E. Byrne: “Myostatin, insulin-like growth factor-1, and leukemia inhibitory factor mRNAs are upregulated in chronic human disuse muscle atrophy.” *Muscle Nerve*. vol. 24, no. 7, pp. 893–899, 2001.
[115] L. Zhang, V. Rajan, E. Lin, Z. Hu, H.Q. Han, X. Zhou, Y. Song, H. Min, X. Wang, J. Du, and others: “Pharmacological inhibition of myostatin suppresses systemic inflammation and muscle atrophy in mice with chronic kidney disease.” *FASEB J.* vol. 25, no. 5, pp. 1653–1663, 2011.
[116] R. Nakao, K. Hirasaka, J. Goto, K. Ishidoh, C. Yamada, A. Ohno, Y. Okumura, I. Nonaka, K. Yasutomo, K.M. Baldwin, and others: “Ubiquitin ligase Cbl-b is a negative regulator for insulin-like growth factor 1 signaling during muscle atrophy caused by unloading.” *Mol. Cell. Biol.* vol. 29, no. 17, pp. 4798–4811, 2009.
[117] J.M. Sacheck, J.-P.K. Hyatt, A. Raffaello, R.T. Jagoe, R.R. Roy, V.R. Edgerton, S.H. Lecker, and A.L. Goldberg: “Rapid disuse and denervation atrophy involve transcriptional changes similar to those of muscle wasting during systemic diseases.” *FASEB J.* vol. 21, no. 1, pp. 140–155, 2007.
[118] S. Clavel, A.-S. Coldefy, E. Kurkdjian, J. Salles, I. Margaritis, and B. Derijard: “Atrophy-related ubiquitin ligases, atrogin-1 and MuRF1 are up-regulated in aged rat Tibialis Anterior muscle.” *Mech. Ageing Dev.* vol. 127, no. 10, pp. 794–801, 2006.

[119] J. Haimes and M. Kelley: “Demonstration of a ΔΔ C q Calculation Method to Compute Relative Gene Expression from qPCR Data.” *Thermo Sci. Tech Note*. pp. 1–4, 2010.

[120] T.M. Randau, F.A. Schildberg, M. Alini, M.D. Wimmer, E.-M. Haddouti, S. Gravius, K. Ito, and M.J. Stoddart: “The effect of dexamethasone and triiodothyronine on terminal differentiation of primary bovine chondrocytes and chondrogenically differentiated mesenchymal stem cells.” *PLoS One*. vol. 8, no. 8, pp. e72973, 2013.

[121] M.A. Wallace, P.A. Della Gatta, B. Ahmad Mir, G.M. Kowalski, J. Kloehn, M.J. McConville, A.P. Russell, and S. Lamon: “Overexpression of striated muscle activator of Rho signaling (STARS) increases C2C12 skeletal muscle cell differentiation.” *Front. Physiol.* vol. 7, pp. 7, 2016.

[122] D. Attaix and V.E. Baracos: “MAFbx/Atrogin-1 expression is a poor index of muscle proteolysis.” *Curr. Opin. Clin. Nutr. Metab. Care*. vol. 13, no. 3, pp. 223–224, 2010.

[123] E.M. MacDonald, E. Andres-Mateos, R. Mejias, J.L. Simmers, R. Mi, J.-S. Park, S. Ying, A. Hoke, S.-J. Lee, and R.D. Cohn: “Denervation atrophy is independent from Akt and mTOR activation and is not rescued by myostatin inhibition.” *Dis. Model. Mech.* pp. dmm–014126, 2014.

[124] X.-H. Liu, W.A. Bauman, and C. Cardozo: “ANKRD1 modulates inflammatory responses in C2C12 myoblasts through feedback inhibition of NF-κB signaling activity.” *Biochem. Biophys. Res. Commun.* vol. 464, no. 1, pp. 208–213, 2015.

[125] S. Kojic, A. Nestorovic, L. Rakicevic, A. Belgrano, M. Stankovic, A. Divac, and G. Faulkner: “A novel role for cardiac ankyrin repeat protein Ankrd1/CARP as a co-activator of the p53 tumor suppressor protein.” *Arch. Biochem. Biophys.* vol. 502, no. 1, pp. 60–67, 2010.

[126] F. Le Grand and M.A. Rudnicki: “Skeletal muscle satellite cells and adult myogenesis.” *Curr. Opin. Cell Biol.* vol. 19, no. 6, pp. 628–633, 2007.

APPENDICES

RCCS OPERATION WITH MICROCARRIERS AND ALGINATE

Lab protocols for operation of the Synthecon RCCS-4H, use of microcarrier beads, and alginate encapsulation are demonstrated in the video linked below. Demonstration and filming by Charles P. Harding, editing by Matt Clegg.

https://usu.box.com/s/pdtf48bzqcyank1mskkg2j1dcefeu7y2